A Three-Dimensional Total Odd Nitrogen (NO_y) Simulation During SONEX Using a Stretched-Grid Chemical Transport Model

Dale Allen[1]

Kenneth Pickering[1]

Georgiy Stenchikov[1*]

Anne M. Thompson[2]

Yutaka Kondo[3]

submitted

Journal of Geophysical Research

March 12, 1999

[1]Department of Meteorology, University of Maryland, College Park, MD 20742

[2]Laboratory for Atmospheres, NASA Goddard Space Flight Center, Greenbelt, MD 20771

[3]Solar-Terrestrial Environment Laboratory, Nagoya University, Honohara, Toyokawa, Aichi 442, Japan

[*]Now at Department of Environmental Sciences, Rutgers-The State University of New Jersey, New Brunswick, NJ 08901

ABSTRACT

The relative importance of various odd nitrogen (NO_y) sources including lightning, aircraft, and surface emissions on upper tropospheric total odd nitrogen is illustrated as a first application of the three-dimensional Stretched-Grid University of Maryland/Goddard Chemical-Transport Model (SG-GCTM). The SG-GCTM has been developed to look at the effect of localized sources and/or small scale mixing processes on the large-scale or global chemical balance. For this simulation, the stretched-grid was chosen so that its maximum resolution is located over eastern North America and the North Atlantic; a region that includes most of the SONEX (the SASS (Subsonic Assessment) Ozone and Nitrogen Oxides Experiment) flight paths. The SONEX period (October-November 1997) is simulated by driving the SG-GCTM with assimilated data from the GEOS-STRAT DAS (Goddard Earth Observing System-STRAT Data Assimilation System). A new algorithm is used to parameterize the lightning flash rates that are needed to calculate emissions of NO_y by lightning. Model-calculated upper tropospheric NO_y and NO_y measurements from the NASA DC-8 aircraft are compared. Spatial variations in NO_y were well captured especially with the stretched-grid run; however, model-calculated concentrations were often too high in the upper troposphere, particularly during the first several flights. The lightning algorithm does a reasonably good job; however, the use of emissions from observed lightning flashes significantly improves the simulation on a few occasions, especially November 3, 1997, indicating that significant uncertainty remains in parameterizing lightning in CTMs. Aircraft emissions play a relatively minor role (~12%) in the upper tropospheric NO_y budget averaged along SONEX flight paths; however, the contribution of such emissions is as large as ~30% during portions of some flights.

1. Introduction

An understanding of the relative contributions of NO_x (NO_x = nitric oxide (NO) + nitrogen dioxide (NO_2)) source terms to the total odd nitrogen (NO_y = NO + NO_2 + NO_3 + HNO_2 + HNO_3 + HO_2NO_2 + $2N_2O_5$ + PAN + other organic nitrate + aerosol nitrate) distribution is essential because of the major role played by NO_x in the production of tropospheric O_3. The most important NO_x source terms in the troposphere are fossil fuel combustion, soil microbial activity, lightning emissions, biomass burning, and dissociation of nitrous oxide (N_2O) in the stratosphere followed by downward transport to the troposphere. The effect of each source term depends on the magnitude of the source but also and perhaps more importantly on its location. Odd nitrogen emitted into the upper troposphere is longer lived than odd nitrogen emitted into the boundary layer and is also more efficient at producing O_3 [*Liu et al.*, 1987; *Hauglustaine et al.*, 1994]. Therefore, upper tropospheric NO_x emissions by lightning and aircraft play a disproportionate role in the NO_y budget. In addition, the importance of lightning and aircraft emissions may increase in the future since both air traffic [*Boeing, 1996; Douglass, 1995*] and global lightning flashes [*Williams, 1992; Price and Rind, 1994*a] are expected to increase over the next several decades.

Estimates of the relative importance of aircraft emissions on upper tropospheric NO_x and NO_y amounts vary widely. *Meijer et al.* [1999] used a three-dimensional chemistry and transport model (CTM) driven by ECMWF (European Centre for Medium-Range Weather Forecasts) fields to study the impact of aircraft emissions on NO_x amounts along four SONEX (the SASS (Subsonic Assessment) Ozone and Nitrogen Oxides Experiment) and POLINAT II (Pollution From Aircraft Emissions in the North Atlantic Flight Corridor (NAFC) II) flight tracks during October 1997. They found that aircraft emissions were responsible for more than 50% of upper

tropospheric NO_x amounts along these flight paths. *Lamarque et al.* [1996] and *Brasseur et al.* [1996] used the three-dimensional IMAGES (Intermediate Model of the Annual and Global Evolution of Species) model to estimate the relative contribution of NO_x source terms on upper tropospheric NO_x in the Northern Hemisphere (NH) midlatitudes. They found that aircraft emissions contribute 20-35% of 200 hPa NO_x; however, they cautioned that their estimates could change significantly as more accurate information on global lightning emissions becomes available. *Flatøy and Hov* [1996] studied the impact of aircraft NO_x emissions on upper tropospheric NO_x and ozone over Europe and the North Atlantic using a three-dimensional mesoscale CTM. They found that NO_x concentrations west of Ireland doubled when aircraft emissions were included. *Hauglustaine et al.* [1994] used a two-dimensional model and estimated that aircraft emissions account for 40-50% of upper tropospheric NO_y concentrations from 30°-60°N. *Kasibhatla* [1993] studied the importance of aircraft emissions using the three-dimensional GFDL (Geophysical Fluid Dynamics Laboratory) CTM. He estimated that aircraft emissions were responsible for 30-40% of upper tropospheric NO_x amounts in the NH midlatitudes (30°-60°N) during April.

The relative importance of aircraft emissions to upper tropospheric NO_x concentrations in and near the NAFC was studied during October and November 1997 as part of SONEX. Odd nitrogen measurements were made on fourteen separate flights during this period. It is difficult if not impossible to determine the contributions from each source using odd nitrogen measurements alone. For example, since most NO_y is emitted as NO, the ratio of NO/NO_y is large when emissions are fresh. Therefore, a high ratio at a remote marine location points to a recent aircraft and/or lightning source. However, the ratio does not provide information on the

importance of contributions from older lightning and/or aircraft emissions. For these reasons and others, a combination of modeling and measurements are needed to ascertain the relative importance of aircraft and lightning emissions. In this study, the relative importance of five source terms: (1) non-aircraft fossil fuel combustion/soil microbial activity, (2) lightning emissions, (3) biomass burning emissions, (4) aircraft emissions, and (5) the stratosphere will be evaluated along SONEX flight paths by solving the three-dimensional constituent continuity equation for NO_y using a CTM with a stretched-horizontal grid (ie., a grid where the spacing between grid points is relatively small and uniform within a region of interest and stretches gradually with latitude and longitude outside of this region) [e.g., *Fox-Rabinovitz et al.*, 1997].

Stretched-grid simulations are useful for looking at the effect of small-scale mixing processes on the larger or global scale chemical balance. An example is mixing in a strong convective storm or after injection from a local source. A relatively high resolution is necessary to simulate the dilution that occurs in the mixing region. A reasonable estimate of dilution is needed because the net O_3 production rate varies nonlinearly with the NO_x concentration [*Chatfield and Delany*, 1990; *Liu et al.*, 1987]. Another example is stratosphere-troposphere exchange, a process which is driven by the large-scale circulation; however, the mixing associated with it occurs at grid scales too small to be resolved explicitly by global models. Stretched-grid simulations are also useful for interpreting measurements taken over limited areas such as those from field studies or aircraft missions. In addition, stretched-grid simulations are useful when high resolution chemical emission data are available over only a portion of the globe.

A major advantage stretched-grid simulations have over nested-grid simulations (ie., simulations where a fine uniform resolution grid is embedded within a coarser uniform resolution

grid) is the lack of lateral boundary conditions. A major advantage stretched-grid simulations have over uniform grid high resolution calculations is that they have less memory and storage requirements and may require fewer computations.

This study serves three main purposes. 1) It describes the development, testing, and application to a scientific problem of the University of Maryland/Goddard Stretched-Grid Chemical-Transport Model (SG-GCTM), 2) it describes a new algorithm to parameterize NO_x emissions by lightning, and 3) it provides NO_y source attribution information for SONEX. The solution of the constituent continuity equation for NO_y is described in section 2 with more information on the advection algorithm in the appendix. The importance of various source terms is highlighted in section 3 which compares model results along the SONEX flight paths with NO_y measurements. The representativeness of the flight paths, the performance of the lightning algorithm, and loss of NO_y by scavenging are discussed in section 4. The results are summarized in section 5.

2. The Chemical Transport Model

The constituent continuity equation for NO_y is solved using the SG-GCTM. The SG-GCTM has been developed for four primary reasons. 1) It allows us to take advantage of chemical emission data that are at a higher resolution than the GEOS-DAS (Goddard Earth Observing System Data Assimilation System) [*Schubert et al., 1993; Bloom et al., 1996*] fields that have been used to drive the tropospheric version of the Goddard CTM (GCTM) *[Allen et al.*, 1996a; *Allen et al.*, 1996b; *Chin et al.*, 1998] in the past. 2) It allows us to focus the resolution on an area where field experiments and aircraft missions have been conducted, 3)

it allows us to test the SG-GCTM before driving it with stretched-grid fields from the stretched-grid GEOS-DAS that is currently under development (*M. Fox-Rabinovitz*, personal communication, 1998), and 4) it allows us to test the advection algorithm used in the SG-GCTM before possibly coupling it with the stretched-grid GEOS-GCM for interactive chemistry/climate forcing calculations *[Fox-Rabinovitz et al.*, 1997; *Fox-Rabinovitz, et al.*, 1999] .

The horizontal grid of the SG-GCTM is chosen by specifying a region of interest where the resolution is highest, a "high" resolution for the region of interest, and a "coarse" resolution for the opposite side of the globe. The location of horizontal grid points is then determined by running a grid generator program *[Fox-Rabinovitz et al.*, 1997]. The spacing between grid points is uniform in the region of interest and increases gradually outside of this region with the maximum spacing being located on the opposite side of the globe.

The region of interest for the stretched-grid SONEX NO_y simulation is chosen to be 100° to 50°W and 25° to 50°N (Figure 1). The grid spacing in the region of interest is 0.9375° in the east-west and 0.75° in the north-south direction (0.9375° x 0.75°) and stretches to 2.5° x 2.0° on the opposite side of the world. The region of interest was chosen to include the region of "high resolution" chemical emission data over eastern North America but extends far enough east to also encompass many of the SONEX flight paths. The "coarse" resolution was chosen to match the resolution of the driving GEOS-DAS. The resolution changes slowly enough that even the easternmost SONEX flights were in an area of relatively fine resolution.

The model has 26 sigma layers (see Table 1) with the lowest 23 being chosen to match the lowest 23 layers of the 46 layer (2.5° x 2.0°) GEOS-STRAT DAS that was used to support the STRAT (Stratospheric TRacers of Atmospheric Transport) and SONEX missions.

Output from the GEOS-STRAT DAS is used to drive the SG-GCTM in an off-line mode. The GEOS-STRAT fields used to solve the continuity equation for NO_y are the u and v components of the wind, the surface pressure, the temperature, the three-hour averaged planetary boundary layer depth, and the six-hour averaged cloud mass flux and detrainment. Since the uppermost three layers of the SG-GCTM do not match GEOS-STRAT layers, the values of fields on these layers are obtained by mapping the GEOS-STRAT fields onto the SG-GCTM layers *(S. J. Lin*, personal communication, 1998). The fields on all layers are interpolated onto the stretched-horizontal grid before use. In the future, we will get our fields from the stretched-grid version of the GEOS-DAS, and this step will be unnecessary. Turbulent and convective mixing are parameterized using algorithms described in *Allen et al.* [1996a, 1996b].

The NO_y simulation was initialized 00 UT July 1, 1997. A 2.5° x 2.0° uniform grid simulation was run through 18 UT September 30, 1997. A stretched-grid simulation was initialized using output from the uniform grid simulation at 18 UT September 30, 1997. Both the uniform and stretched-grid simulations were run through 18 UT November 14, 1997.

2.1. Stretched-grid advection scheme

The mixing ratio change due to advection was calculated by modifying *Lin and Rood's* [1996; *LR96* hereafter] multidimensional and semi-Lagrangian extension of the piecewise parabolic method (PPM) *[Colella and Woodward*, 1984] for use on a non-uniform grid. This is the first application of a semi-Lagrangian scheme on a non-uniform grid. A semi-Lagrangian approach is appealing for stretched-grid calculations because the time step needed to maintain stability with Eulerian schemes is limited by the resolution in the high resolution area. The advantage of semi-Lagrangian schemes is that there is no restriction on the time step. Therefore,

a time step appropriate for the physical processes being simulated can be chosen. We chose a time step of twelve minutes for this simulation. The advection algorithm is described in some detail in the appendix. The major changes from *LR96* are:

1. The semi-Lagrangian extension is invoked automatically in both the north-south and east-west directions whenever the CFL (Courant-Friedrichs-Levy) condition is violated. *LR96* automatically invoke the semi-Lagrangian extension in the east-west direction at high latitudes. 2. The second order PPM of *Colella and Woodward* [1984] is used for horizontal advection. *LR96* use a fourth order version of the PPM. 3. The calculation of the Courant number at grid points where the CFL condition is violated is more complex because of the nonuniform grid. 4. The PPM is used to calculate the "fractional flux" for the semi-Lagrangian extension (see appendix). *LR96* used van Leer's algorithm [*van Leer*, 1979] for this extension. This change was for convenience only and is not expected to increase the accuracy of the overall approximation.

2.2 Specification of NO_y Sources and Sinks

Five different sources of NO_y are included in the simulation. They are fossil fuel/soil NO_y, lightning NO_y, biomass burning NO_y, aircraft NO_y, and stratospheric NO_y. The contribution to total NO_y of each of the five source is calculated separately. The algorithms used to specify each of the five sources are now described.

2.2.1. Fossil fuel/soil NO_y. An emission inventory for fossil fuel/soil emissions of NO_x was obtained by merging NO_x emissions from the OTAG (Ozone Transport Assessment Group) *[OTAG*, 1997a; *OTAG*, 1997b] and GEIA (Global Emissions Inventory Activities) *[Benkovitz et al.*, 1996; *Yienger and Levy*, 1995] inventories. The high resolution (0.5° x 0.33°) OTAG inventory is used over the eastern United States (99°-67°W, 26°-47°N) while the 1° x 1° GEIA

inventory is used over the remainder of the globe. The OTAG inventory includes both soil and fossil fuel emissions and is divided into high-level point and area sources. The OTAG inventory used in this simulation was developed for July 7-18, 1995. The average daily emissions for July 7-13, 1995 are used in this simulation. The OTAG emissions at each grid point are adjusted to ensure that the total global emission of the combined OTAG/GEIA inventory matches the total global emission of the GEIA inventory for that month. This adjustment is necessary because the magnitude of the OTAG source is appropriate for July 7-13, 1995 while July-November, 1997 is simulated. Emissions by high-level point sources are put into the second model layer, while emissions by area sources are put into the lowest model layer.

Separate GEIA inventories are used for fossil fuel combustion *[Benkovitz et al.*, 1996] and soil-biogenic emissions [*Yienger and Levy*, 1995]. The fossil fuel inventory is divided into high (>100m) and low level emissions. The fossil fuel inventory is available for each season, while the soil-biogenic inventory is available monthly. Emissions by high-level sources are put into the second model layer, while emissions by low level sources and the soil are put into the lowest model layer.

2.2.2. Lightning NO_y. NO_x is produced via the Zel'dovich mechanism *[Zel'dovich and Raizer*, 1966] during lightning flashes. The mass of NO_x produced per flash is related to the energy of each flash. *Y.-J. Wang et al.* [1998] have reported that the NO_x production per unit energy is a nonlinear function of flash energy. However, because we do not have global information on flash energies we follow *Price et al.* [1997a] and assume that the NO_x production per unit energy is constant. Therefore, the total mass of nitrogen (N) in NO produced per second (G) is given by

$$G = (f_{CG} * LF * E_{CG} + (1-f_{CG}) * LF * E_{IC}) * P * CONV, \quad (1)$$

where f_{CG} is the fraction of total flashes that are cloud-to-ground, LF is the total flash frequency (flashes s^{-1}), E_{CG} is the mean energy of a cloud-to-ground flash (Joules(J)), E_{IC} is the energy of an intracloud flash (J), P is the mean NO production rate per unit energy (molecules NO/J), and CONV is a conversion factor equal to the molecular weight of N (14 g/mole) divided by Avogadro's number ($6.02X10^{23}$ molecules/mole).

Following *Price et al.* [1997a], P is assumed to equal 10 x 10^{16} molecules NO/J, E_{CG} is assumed to be 6.7 x 10^9 J, and E_{IC} is assumed to equal 0.1* E_{CG}. However, estimates of P range from 5-15 x 10^{16} molecules [*Price et al.*, 1997b], while estimates of the ratio of E_{IC} to E_{CG} range from 0.1 to 0.33 or more [*Price et al.*, 1997a; *Gallardo and Cooray*, 1996]. The fraction of total flashes that are cloud-to-ground (f_{CG}) can be related to the thickness of the cloud above the freezing level (cold-cloud thickness) [*Price and Rind*, 1993],

$$\begin{aligned} f_{CG} &= 0. && \Delta z < 5.5, \\ f_{CG} &= 1./[(A\Delta z^4+B\Delta z^3+C\Delta z^2+D\Delta z+E)+1] && 5.5 \le \Delta z \le 14, \\ f_{CG} &= 0.02 && \Delta z > 14, \end{aligned} \quad (2)$$

where A = 0.021, B = -0.648, C = 7.493, D = -36.54, E = 63.09, and Δz is the depth (km) of the cloud above the freezing level. In the SG-GCTM, the cloud top is assumed to equal the pressure at the top edge of the uppermost layer that has nonzero convective mass flux across its bottom edge. The cold-cloud thickness (Δz) is calculated by starting with the top cloud layer and summing the depths of each layer below it until a layer is reached for which the T > 273K.

The total flash frequency (LF) was not calculated during the GEOS-STRAT assimilation. Therefore, a parameterization in the CTM is necessary. *Price and Rind* [1992] provide a method

of estimating flash rates using cloud top height. When we applied this method for the SONEX period we found that it severely underpredicted cloud-to-ground flashes over the Atlantic Ocean. The Price and Rind marine flash rate formula did not appear to be valid for a region of relatively strong instability such as over the warm waters of the Gulf Stream. This finding is consistent with the results of *Gallardo and Rodhe* [1997]. They found that their model-calculated distribution of total nitrate in the remote Pacific improved when they increased their marine lightning flash rates significantly from values obtained using the Price and Rind marine formulation. In addition, because of the algorithm used in the SG-GCTM to calculate cloud top heights, the model cloud top heights were bunched about the mean height of each model layer. Because of this, for a given cloud top height a wide range of observed flash rates occurred, making cloud top height from the model a rather poor predictor of flash rate. Therefore, we have developed a preliminary version of an alternative method for estimating the flash rate using six-hour averaged convective mass fluxes from the GEOS-STRAT assimilation. The magnitude of these fluxes is related to the intensity of deep convection. Since the intensity of deep convection (e.g., upward vertical velocity) is related to the lightning flash rate *[MacGorman and Rust*, 1998; *Baker et al.*, 1995; *Pickering et al.*, 1998], an empirical relationship between the mass flux and the flash frequency can be determined and used to parameterize the flash frequency. Cloud-to-ground lightning flash rates for 10°-70° N and 180°-0° W on a 1° x 1° grid are currently available through the National Lightning Detection and Long Range Flash Networks (NLDN/LRF) *[Wacker and Orville*, 1999; *Cramer and Cummins*, 1998]. The actual cloud-to-ground flash rate is believed to be higher because the network is not 100% efficient in detecting lightning flash rates. Because of this, the measured flash rates are adjusted by dividing by the detection

efficiency before being compared to the GEOS-STRAT mass fluxes. The detection efficiency was estimated using a 4th order polynomial determined with the constraints that the efficiency equals 0.9 over the United States of America (US), 0.6 at a distance of 1000 km from the US, 0.3 at a distance of 2000 km from the US, and 0.15 at distances greater than 3000 km from the US coast *(S. Goodman*, personal communication, 1997). Diurnal variations in detection efficiency were not considered. Since the detection efficiency is imprecise (the above values are best case estimates), only grid points relatively close to the US (10°-60°N and 120°-60°W) were used to determine the empirical relationship. The adjusted NLDN/LRF flash rates are averaged over the same six hour periods as the mass fluxes and aggregated into the 2.5° x 2.0° GEOS-STRAT grid boxes. The adjusted flash rates for November 1-9, 1997 were then sorted by magnitude. Similarly, the GEOS-STRAT mass fluxes at 0.44 sigma (≈440 hPa) for the same period were sorted by magnitude. The choice of 0.44 sigma limits lightning production to deep convective clouds (ie., clouds with a cloud top of ≤ 440 hPa). The sorted NLDN/LRF flash frequencies after adjusting for detection efficiency are plotted versus the sorted 0.44 sigma mass fluxes in Figure 2. A fourth order polynomial was fit to the sorted fields (after converting to per minute) assuming the mass flux was the independent variable and the lightning flash rate the dependent variable. The resulting cloud-to-ground flash rate becomes:

$$LF_{CG} = a + bM + cM^2 + dM^3 + eM^4 \qquad (3)$$

where a = -0.7133, b = 2.3450, c = -2.5104, d = 0.9568, e =-0.0564, LF_{CG} is the cloud-to-ground flash rate (flashes min^{-1}) within the 2.5° x 2.0° grid box, and M is the cloud mass flux (kg $m^{-2} min^{-1}$). The polynomial gives unrealistic flash rates for M ≥10 kg $m^{-2} min^{-1}$. Therefore, it is not appropriate for use with a mesoscale model where larger mass fluxes are possible;

GEOS-STRAT mass fluxes rarely exceed 6 kg m^{-2} min^{-1}. Separate fits were initially tried for land and water points; however, the fits were similar so land and water points were combined. The number of grid points with nonzero mass fluxes exceeded the number of grid points with nonzero observed flash rates. After sorting, it was found that mass fluxes less than 0.55 kg m^{-2} min^{-1} had flash rates of zero associated with them. Therefore, the lightning flash rate for mass fluxes less than 0.55 kg m^{-2} min^{-1} was automatically set to zero. The resulting cloud-to-ground flash rate (LF_{CG}) is appropriate for a 2.5° x 2.0° grid box at 30°N latitude. The total flash rate in a grid box (LF) can be obtained by multiplying LF_{CG} by the area of the grid box ($\Delta x \Delta y$) and dividing by the cloud-to-ground fraction (f_{CG}) and the area (A) of a 2.5° x 2.0° grid box at 30° latitude ($\approx 5.35 \times 10^{10}$ m^2). Mathematically,

$$LF = \Delta x \Delta y LF_{CG} / (f_{CG} A), \quad (4)$$

where LF_{CG} and f_{CG} are the cloud-to-ground flash rate (Equation 3) and the cloud-to-ground fraction (Equation 2), respectively, after interpolating onto the stretched grid. The interpolation of f_{CG} onto the stretched-grid can result in extremely small values of f_{CG} which can in turn produce unrealistically large amounts of intracloud lightning. Because of this, the flash rate is set to 0 for $f_{CG} < 0.01$. The NO production rate is now found using equation 1.

Stretched-grid and uniform-grid experiments were also run where the parameterized flash rates (LF_{CG}) between 20°-60°N and 130°-50°W for October 9 through November 12 were replaced by the NLDN/LRF flash rates after adjusting for efficiency. A difficulty with this simulation is that the observed flashes and GEOS-STRAT deep convection are not always aligned. In other words, lightning flashes may occur at grid points where deep convection did not occur in the model, and the cloud top pressure is undefined. For these simulations, the cloud

top pressure in regions where observed flashes are used was assumed to equal the pressure at the top of the uppermost layer entirely within the troposphere. The tropopause pressure (P_{trop}) is defined to be the largest pressure (P< 500 hPa) at which the GEOS-STRAT Ertel potential vorticity [*Ertel*, 1942] equals 2.5 x 10^{-6} K m^2 kg^{-1} s^{-1}. If the resulting tropopause pressure is less than the pressure at the 380 K surface, the pressure at the 380 K surface is used as the tropopause pressure (*S. Steenrod*, personal communication, 1998). This cloud top pressure is then used to calculate Δz in the formula for f_{CG} (Formula 2).

The final step in the lightning NO_x parameterization is to determine what fraction of the total emissions to put into each layer. This step is also important. *Lamarque et al.* [1996] found that the relative contribution of lightning NO_x to the NO_x budget changed by 10-20% when they changed the vertical distribution of lightning NO_x in the IMAGES CTM. *Pickering et al.* [1998] constructed vertical profiles of lightning NO_x emissions for tropical continental, midlatitude continental, and tropical marine conditions. The profiles of *Pickering et al.* [1998] need to be scaled to the heights of the clouds in the SG-GCTM. We adjusted the emission heights using the cloud top height at each SG-GCTM grid point and then interpolated the emissions onto the heights of the SG-GCTM layers. The fractions were then adjusted in order to ensure that the sum of the fractional emissions into all the model layers equals one. The tropical continental (marine) profile was used in the SG-GCTM at all model grid points over land (ocean) within 30° of the equator. The midlatitude continental profile was used at all SG-GCTM grid points (land or ocean) poleward of 30°.

2.2.3. Biomass burning NO_y. NO_x emissions from tropical and sub-tropical biomass burning are calculated using monthly 5° x 5° data sets of total biomass burned from deforestation and

shifting cultivation, savanna burning, fuelwood burning, and agricultural residue burning [*Hao et al.*, 1994]. Burning from deforestation, savannas, fuelwood, and agricultural residues are assumed to emit 0.0025, 0.0020, 0.0015, and 0.0010 tons of nitrogen (N) per ton of biomass burned respectively [*Dignon and Penner*, 1991]. NO_x emissions from midlatitude and high latitude biomass burning are not included in the simulation. All emissions by biomass burning are put into the lowest layer of the model.

2.2.4. Aircraft NO_y. Monthly average aircraft NO_x emissions based on 1992 scheduled air traffic have been generated on a 1° longitude by 1° latitude by 1 km pressure altitude grid by *Baughcum et al.* [1996]. NO_x emissions from this twenty-one layer inventory were used in this simulation. The emissions from each of the twenty-one layers were put into the appropriate SG-GCTM layer by comparing the emission pressure from the inventory with the pressures at the edges of each SG-GCTM layer. The SG-GCTM surface pressure was assumed to equal 1000 hPa during this comparison. The resulting emission distribution was interpolated onto the SG-GCTM grid.

The *Baughcum et al.* [1992] inventory did not include diurnal variability. However, flights in the Organized Track System (OTS) within the North Atlantic (defined here to be 10°-60°W, 45°-60°N) are not uniformly distributed throughout the day *[Schlager et al.*, 1997]. Most departures from North America occur in the evening (23 UT-4 UT) and reach Europe the following morning (5 UT-8 UT) while most departures from Europe occur in the early afternoon (12 UT-15 UT) and reach North America in the early-mid afternoon (16 UT-18 UT). This diurnal variability was added to aircraft emissions in the NAFC (see Table 2).

2.2.5. Stratospheric NO_y. The stratospheric NO_y simulation was initialized using 00 UT July 1, 1997 output from a calculation in support of the POLARIS (Photochemistry of Ozone Loss in

the Arctic Region in Summer) mission using the full stratospheric chemistry version of the GCTM *[Douglass et al.*, 1997, 1999]. The 2.5° x 2.0° "POLARIS" simulation was initialized March 20, 1997 and run on 28 vertical layers. The 28 layer output was interpolated onto the 2.5° by 2.0° by 26 layer grid. The NO_y mixing ratio was set to zero at all grid points where the pressure exceeded the tropopause pressure. The initialization with model output as opposed to climatological measurements minimized the amount of cross-tropopause flow that occurred as the NO_y simulation spun up.

The primary production mechanism for NO_y is dissociation of N_2O in the stratosphere. This production is parameterized using production coefficients from the Goddard two-dimensional model *[Jackman et al.*, 1996].

When interpreting the relative importance of NO_y source terms, it is important to remember that stratospheric NO_y in this simulation includes both NO_y that was in the stratosphere as of 00 UT July 1, 1997 and NO_y that was produced after that date by dissociation of N_2O in the stratosphere. Therefore, stratospheric NO_y also includes NO_y that originated via surface sources, lightning emissions, or aircraft emissions prior to July 1 and was transported to the stratosphere.

2.2.6. Dry Deposition and Wet Scavenging. Loss by dry deposition and wet scavenging of NO_y are simulated as a first order loss process dependent on altitude [*Logan et al.*, 1981] and surface type (land, water, ice). The resulting lifetimes as a function of altitude and underlying surface (land, water, or ice) are shown in Table 3. The NO_y lifetimes have been adjusted in the mid-and-upper troposphere to account for loss due to ice particle scavenging and settling [*Lawrence and Crutzen*, 1998]. Land (ocean) points poleward of 50°(70°) are assumed to be ice covered if the

temperature in the lowest model layer is less than 268K.

2.2.7. Total emissions. The total global emissions (expressed as an annual mean) from each NO_y source for the last six weeks (October 1-November 14, 1997) of the simulation are shown in Table 4. The fossil fuel/soil and biomass burning terms dominate although their influence is mitigated by the fact that they are subjected to larger loss processes since they are emitted into the lowest two layers of the model. The magnitude of the October-November lightning source (3.6 Tg N/yr) is within the range of recent annual estimates of 3-5 Tg N/yr by *Levy et al.* [1996] but lower than the 12-13 Tg N/yr estimated by *Price et al.* [1997a; 1997b].

3. Model simulation results

Four separate experiments were run for the SONEX period as listed below:

UGPL: Uniform 2.5° x 2.0° grid with parameterized lightning

SGPL: Stretched grid with parameterized lightning

UGOL: Uniform 2.5° x 2.0° grid with observed lightning for 20°-60°N and 130°-50°W

SGOL: Stretched grid with observed lightning for 20°-60°N and 130°-50°W

The results of these simulations are discussed in terms of several specific SONEX flights of the NASA DC-8 aircraft. Model output was saved every six hours and was then sampled at the latitudes, longitudes, and altitudes of 60-s averaged NO_y measurements along the DC-8 flight tracks. The sampled data from the model were interpolated linearly to the times of specific observations. We discuss results for flights from the three bases of operation during SONEX (Shannon, Ireland; the Azores; and Bangor, Maine). Flight paths for the flights discussed in this paper are shown in Figure 3.

3.1. Flight 7 - October 23, 1997

This flight of the DC-8 was designed to characterize the air in the Organized Track System (OTS) of the NAFC after the early morning peak in the eastbound air traffic. The flight was conducted to the north of Ireland and cross-track flight legs were flown at altitudes ranging from 7.6 to 11.2 km (see Figure 3). Figure 4a,b shows the measured NO_y, as well as the simulated NO_y from the five different sources for Experiments UGOL and SGOL. The contribution to NO_y from aircraft is the greatest at the two highest altitudes flown by the DC-8, up to ~125 pptv or ~25-30% of the total NO_y in Experiment SGOL. Averaged over the entire flight, the model estimate of the aircraft contribution was 15%. However, there is uncertainty associated with this estimate because it was obtained using monthly averaged aircraft emissions apportioned according to estimated diurnal variation of air traffic in the NAFC. A more detailed day-by-day inventory for SONEX that includes emissions from the specific aircraft flying in the corridor will be available in the future.

We note that a considerable high bias exists in the model results throughout much of this flight, with the exception of two intervals during the higher altitude portion of the flight. The bias is somewhat less in Experiment SGOL (stretched-grid) than for Experiment UGOL. The high bias was also noted particularly on the other flights from Shannon and on the transit flights to Shannon from Moffett Field, CA. We speculate that this results from the use of a first order loss process for NO_y rather than episodic removal in individual precipitation systems including scavenging in convective updrafts (see section 4.3). Such removal mechanisms may reduce the upper tropospheric contribution of fossil fuel and soil NO_y. If this is the reason for the high bias, the aircraft contribution to NO_y on this flight may have been greater than ~25-30% at the highest

altitudes and 15% averaged over the entire flight. The model results do show a substantial fossil fuel/soil source contribution on this flight. In addition, trajectory-based convective influence calculations using dynamical fields from the GEOS-STRAT DAS [*Thompson et al.*, this issue] show some exposure of the air sampled on this flight to convection over the previous 5 days.

Analyses of combinations of tracers and probability distributions of the observed data showed that relatively fresh aircraft plumes accounted for 6-12% of the NO_y measured on this flight [*A. M. Thompson*, personal communication, 1999]. Analysis of the data alone cannot provide an estimate of the total aircraft contribution because no unique tracer of aircraft emissions exists that would allow identification of the more aged emissions. Therefore, our model simulation aids in the interpretation of this flight and suggests that the total aircraft contribution to NO_y to be perhaps at least twice the contribution from the identified fresh emissions.

3.2. Flight 9 - October 28, 1997

Figure 5a,b shows model results (Experiments SGPL and UGOL) compared with observations for the flight from Shannon to the Azores (see Figure 3). The model (Experiment SGPL) produces a broad peak from 1300 to 1445 UT that is of the same magnitude as the two observed peaks at 1345 and 1415 UT. The model suggests a substantial stratospheric contribution to the observed NO_y in the first peak. Experiment SGPL also shows an enhanced lightning contribution near the time of the second observed peak. In contrast, Experiment UGOL (uniform grid, observed flashes) did not produce a peak as high as the two observed maxima and it did not overlap them in time as well as Experiment SGPL. Therefore, our lightning flash parameterization appears to yield better results than use of the observed flashes in this case. This result may be due to large uncertainty in the detection efficiency of flashes over the ocean.

Experiment SGPL well simulates the minimum observed values between 1445 and 1545 UT and the maximum from 1600 to 1645 UT. During both of these features the model suggests that the NO_y is largely from the fossil fuel and soil source, but with a 34% lightning contribution in the peak. In Experiment UGOL the model had a high bias during these periods and contained a larger lightning contribution. The model in all four experiments overestimated the observed mixing ratios during the 1645-1730 UT minimum and 1730-1815 UT maximum, which again were dominated by fossil fuel and soil emission along with a significant lightning contribution. The model nearly perfectly captured the time and location of this minimum and maximum; however, the final observed peak at 1845 UT was missed by the model in all four experiments. Substantial convective influence and lightning exposure at points along this flight are suggested by the trajectory-based products described by *Thompson et al.* [this issue], in agreement with our NO_y simulations.

3.3. Flight 10 - October 29, 1997

Figure 6a,b displays the model results (Experiments SGPL and UGOL) and observed NO_y for the October 29 flight to the south of the Azores (see Figure 3). A cut-off low existed in the flow near the Azores, and both the observations and the model show NO_y peaks near the beginning of the flight (~1200 UT). The model shows that, as expected, stratospheric NO_y made a large contribution to this peak. Experiment SGPL (stretched grid) performed better in capturing the structure of this peak, while the uniform grid model (Experiment UGOL) better simulated the magnitude of the peak. Overall Experiment SGPL better simulated the magnitude and structure of the mixing ratios between 1230 and 1630 UT. During this time period significant lightning contributions were evident (up to ~50% of the total NO_y using the observed flashes). The

enhancements in the lightning contribution were stronger in Experiment UGOL than in Experiment SGPL. The stronger lightning signal in the run using observed flashes better explained the observed NO_y maximum between 1400 and 1500 UT, but also produced peaks not seen in the observed NO_y at 1300 and 1345 UT.

The model did not perform particularly well for the return to the Azores at the end of the flight. A peak in the NO_y observations (averaged to 60 s intervals) reaching to nearly 2 ppbv at ~1700 UT was followed by an approximately 1-hr period of mixing ratios of ~1 ppbv. The model produced a lightning peak at ~1645 UT, which was the strongest in Experiment UGOL, and a large stratospheric peak from 1715 UT to the end of the cruise altitude part of the flight. It is possible that the model lightning peak was offset slightly in time and space and corresponds to the nearly 2 ppbv maximum. Experiment SGOL (stretched grid, observed flashes) produced a peak even more closely reaching this observed maximum. It is likely that the sustained 1 ppbv period indicates reentry into the cut-off low near the Azores. All of the model experiments overestimate the stratospheric contribution during this period.

The stretched-grid simulations are also useful for determining the origin of lightning NO_y. For example, a large amount of the lightning NO_y observed on October 29th near the Azores appears to have been emitted over the southeastern United States during thunderstorms on October 26th and 27th (see Figures 7a-d). Model-calculated lightning NO_y concentrations from experiment SGOL at 250 hPa exceeded 2.5 ppbv over central Florida on October 27th. The lightning NO_y was transported across the Atlantic and had nearly reached the October 29th flight track as of 12 UT October 29th.

Analyses using trajectory-based model products that use winds and temperature from the

GEOS-STRAT assimilation are described in *Thompson et al.* [this issue]. The 29 October 1997 flight is one of two discussed in detail in that paper. The RDF (reverse-domain fill) plot of potential vorticity at 330 K put the cut-off low over the Azores, where high NO_y was encountered on the takeoff and landing parts of the flight. Several different approaches were tried with convective and lightning influence. These show maxima at the location of the high NO_y at 1400-1500 hours (Figure 6a). The back-trajectory (product BT in *Thompson et al.* [this issue]) from 1400-1500 hour originates from convective activity and lightning *[Pfister et al.*, this issue] over the northeast United States and maritime Canada. Tracers such as CO, HC etc. are consistent with the trajectory implications. However, this result is not consistent with our lightning NO_y simulation, which shows lightning over the southeastern United States as the primary contributor. Both approaches use the same wind data; however, the trajectory-based products result from a Lagrangian technique using the isentropic assumption, while our NO_y simulation results from a largely Eulerian technique using kinematically-computed vertical velocities.

The observed peak in NO_y at 1700 hours (Figure 6a) which is also suggested by the convective and lightning exposure plots [*Thompson et al.*, this issue] is more ambiguous when one looks at the tracers. *Davis et al.* [this issue] argue for aircraft influence which is supported by a maximum in aircraft exposure [*Thompson et al.*, this issue]. Our NO_y simulations (particularly the SGOL Experiment) however, suggest a lightning source for the 1700 UT peak.

3.4. Flight 12 - November 3, 1997

The first SONEX flight from Bangor, Maine was conducted primarily along the coast of Newfoundland and Labrador but north of the OTS westbound air traffic (see Figure 3). Figure 8a,b shows model (Experiments UGOL and SGOL) and observed NO_y for this flight. These

experiments (using the observed flashes) came much closer to matching the observed NO_y than did the parameterized flash runs (Experiments UGPL and SGPL) for this flight. Experiment SGOL (stretched grid) performed better than Experiment UGOL for the early part of the flight (1330 - 1515 UT). During this period a mix of all of the sources appears to have contributed to the total NO_y. The observed peak at 1445 UT corresponds to a maximum in the fossil fuel and soil source contribution. Between 1515 and 1930 UT Experiment UGOL produced NO_y mixing ratios that better agreed with the peak observed values, but the coarser-grid simulation results lack the large variability seen in the observations. Lightning and fossil fuel sources dominated the large peaks occurring at ~1600 and ~1700 UT. *Pickering et al.* [this issue] show that these maxima may represent outflow from convection approximately 1.5 days upstream over the southeastern United States. Lightning was the predominant source for the 1830-1930 UT peak, which likely resulted from marine convection not far south of the flight region *[Pickering et al.*, this issue]. The Experiment UGOL and SGOL results show up to ~60-65% of the NO_y may be from lightning during this period. The trajectory-based lightning exposure and convective influence products *[Thompson et al.*, this issue] show that air parcels in the region of the 1830-1930 UT Peak (central Newfoundland to northern Nova Scotia) passed through grid cells containing lightning (some parcels up to ~100 flashes). The transport time to the most recent convection for these parcels ranged from 0-8 hours to 24-32 hours. During the remainder of the flight the stretched grid simulation (Experiment SGOL) more closely matched the observed NO_y.

3.5. Flight 14 - November 9, 1997

The DC-8 sampled the OTS along the Newfoundland coast soon after the peak of the westbound air traffic on this date (see Figure 3). Figure 9 presents the observations and the model

results for Experiment SGPL (stretched grid, parameterized flashes). All of the simulations were much lower than the observations for almost the entire flight, and the simulations using observed flashes showed even greater underestimates. Flight legs at five altitudes were flown across the OTS. The largest aircraft contribution to NO_y (~20%) is seen at the highest altitude (11.3 km) in Experiment SGPL. *Pickering et al.* [this issue] and *Jeker et al.* [this issue] show that extensive marine convection containing frequent lightning occurred upstream on this day, suggesting a lightning source for much of the enhanced NO_y detected on this flight. The parameterized flash simulations showed the largest lightning contributions to total NO_y (up to 60% for the 1845 - 1900 UT maximum); however, all of our model experiments appear to underestimate the downstream effects of these lightning flashes.

Several factors may contribute to the underestimation. The lightning flashes downwind of the November 9th NO_y peaks appear to have occurred ~500-1000 km from the coast. The efficiencies we used to calculate lightning emissions were theoretical best case scenarios that based on very recent experimental data appear to have been much too optimistic. *Cramer and Cummins* [1998] estimated lightning flash rates over Kansas and Oklahoma using local sensors and compared the estimates to flash rates obtained using only sensors on the east and west coasts on the United States. The efficiency at ~1400 km was only ~15% during the night and ~5% during the day. Experiment SGOL was rerun for November 7-11th using detection efficiencies based on the recent experimental data. The overall contribution of lightning emissions along the November 9th flight track increased from 42 to 62%; however, total NO_y amounts were still much lower than observed and never exceeded 1.5 ppbv. Measured NO_y concentrations exceeded 2 ppbv during a significant portion of the flight path and were as high as 3.5 ppbv. It is possible that the

intracloud flashes upstream of this flight were more energetic than we assumed in our algorithm. Our assumption that intracloud flashes have one-tenth of the energy of cloud-to-ground flashes is on the low end of values used in recent simulations. For example, *Wang et al.* [1998] assumed intracloud flashes have one-third the energy of cloud-to-ground flashes while *Gallardo and Cooray* [1997] estimated the ratio to be closer to one-to-one. In addition, recent field observations and cloud-scale modeling for a Colorado storm (*DeCaria et al.*, manuscript in preparation) suggest a ratio of energies of approximately one half. Use of this ratio would bring our model-estimated NO_y for this case closer to the observations.

This is the second case study featured in the *Thompson et al.* [this issue] and *Pfister et al.* [this issue] discussions of trajectory-based model products. Comparison of exposure plots confirms the lightning and convective influence which appeared throughout most of the flight with varying degrees of continental and maritime signatures in the tracers. The lightning exposure products show the highest values on the 325 K isentropic surface to be between 62°W and 70°W (the longitudes of the transit legs outbound and inbound to Bangor). This coincides with high NO_y (Figure 9); NO/NO_y ratios were observed at 0.4-0.7 during these periods. The northern and southern ends of the cross-track section are prominent in the lightning exposure product at 331 K; the southern end is the location of the highest NO_y in the flight between 1830 and 1930 UT, where our NO_y simulation shows up to 60% from lightning. Transport time was less than 24 hours from the most recent convection for almost all air parcels showing convective influence. Many air parcels (particularly those at 325 K) had only been transported 0-8 hours from convection. Aircraft influence appears to be present as sharp spikes in the 1-s NO_y time series [*Pickering et al.*, this issue] and as the tail of the distribution function for this flight [*Thompson*

et al., 1999], but it cannot be fingerprinted with tracers. In this case, a more refined model treatment with a finer grid than used in the present study and with the emission inventory based on the actual aircraft traffic appears to be the best approach to further analysis of the aircraft influence.

3.6. Summary of Source Contributions for All SONEX Flights

We have averaged the model-computed NO_y mixing ratios attributable to each source over each SONEX flight, and results for Experiment SGPL are shown in Figure 10a. The average percentage contribution made by each source is shown in Figure 10b. Aircraft contributions range from ~6% on the October 28 flight from Shannon to the Azores to ~17% on the November 10 flight to the northwest of Bangor. The model estimates the lowest average NO_y for the November 10 flight, with the fossil fuel/soil source only contributing ~120 pptv. The cross-track flights (Oct. 18, Oct. 23, and Nov. 9) did not show particularly enhanced aircraft contributions. This result is likely due to the fact that we did not have a detailed aircraft emission inventory specific to the days in question.

Stratospheric contributions ranged from 12% on the November 9 flight in the OTS along the coast of Newfoundland to 53% on the October 25 flight to the north of Shannon along the coast of Norway. The November 9 case was the flight most dominated by the lightning source (at least ~42% and perhaps ~62% or more). Substantial lightning contributions were also found on the flights of 13, 23, and 28 October and 3 November.

Source contributions averaged over all of the SONEX flights are shown at the tops of Figures 10a (mixing ratios) and 10b (percentages). The fossil fuel/soil source dominated with an average 40% contribution. Uncertainty exists in this estimate because of the high bias

(particularly during the first several flights) that may be due to not removing NO_y episodically in precipitation. If this is true, the contribution from fossil fuel/soil may be lower and the other sources proportionally higher. The overall aircraft source contribution was estimated at 12%, substantially lower than the contributions from the stratosphere and lightning (26% and 20%, respectively). Our estimate of the aircraft contribution is similar to that reported by *Friedl et al.* [1997] using four different CTMs. These models estimated the zonal mean contribution of aircraft to total NO_y in the upper troposphere at northern midlatitudes is about 10% in summer and 15% in winter.

Thompson et al. [1999] assigned likely NO_y sources on the basis of clustering of subsets of flights based on probability distributions of NO_y and other tracer mixing ratios. How do the CTM-based budgets compare? We look at this in terms of the budget as a whole (summarized in Figure 10b) and in terms of selected individual flights. In order to be consistent with *Thompson et al.* [1999] we will only consider NO_y with a non-stratospheric source. *Thompson et al.* [1999] assigned 15% of air parcels sampled during SONEX as stratospheric, based on a criterion of ozone > 100 ppbv. We assigned 26% of parcels as stratospheric based on the CTM labeling. Of upper tropospheric air parcels on all SONEX flights, *Thompson et al.* [1999] use tracer ratios to infer that ~40% of NO_y has not reached a statistically predominant mixing ratio characteristic of background air. This fraction is presumed due to relatively fresh NO_x emissions from aircraft, lightning and recent convective transport. The total NO_y budget in Figure 10b, if only non-stratospheric sources are considered, consists of ~42% aircraft plus lightning, similar to the tracer and statistical analysis of *Thompson et al.* [1999].

How do individual cases compare? Take for example, the continental mid-latitude category

of *Thompson et al.* [1999], which is used to describe flights with the most polluted and aged air parcels (NO_y mean mixing ratio close to the most probable mixing ratio and low NO/NO_y). These are 28 and 31 October 1997 and 5, 10, and 12 November 1997. From Figure 10b, it can be seen that ~55% of the non-stratospheric NO_y from these flights is from fossil fuel/soil sources, as expected from continental mid-latitude sources. For these cases, approximately 19% of the CTM-labeled tropospheric NO_y is from aircraft, a significant fraction. This is a conclusion that cannot be made from consideration of the observations alone. Consider the lightning-dominated flights identified in *Thompson et al.* [1999]: 13 and 29 October 1997, 3 and 9 November 1997. Our labeled CTM study suggests that ~37% of non-stratospheric NO_y derives from lightning averaged over all of these cases except 29 October, for which lightning NO_y accounts for ~24% and the fossil fuel/soil source is ~53%. The difference between the October 29th and November 9th flights is not apparent from the NO_y PDFs (probability distribution functions) for those flights [*Thompson et al.*; 1999] . The PDFs are nearly identical with each showing a peak at ~170 pptv and a relatively large tail extending beyond 1500 pptv. Reactive nitrogen on the November 9th flight appears to be predominantly from lightning along with a mixture of marine and anthropogenic signatures in convection [*Pickering et al.*, this issue; *Snow et al.*, this issue]. Lightning network and satellite cloud images show areas in and south of the 9 November sampling region to have intense convective activity.

The five SONEX flights (non-stratospheric portions) between 15 and 25 October 1997 were classified by *Thompson et al.* [1999] as two with dedicated cross-track sampling and three with subtropical origins. All of them are rather similar in NO_y PDFs, and have a strongly peaked CO mixing ratio between 60-70 ppbv, which is 10-30 ppbv lower in CO than the more polluted, mid-

latitude-influenced air parcels. The subtropical designation for the 15, 20, and 25 October flights would be consistent with the 20-25% lightning NO_y source that appears in Figure 10b because trajectory-based convective exposure model products *[Thompson et al.*, this issue; *Pfister et al.*, this issue] show these flights to be influenced by convection/lightning sources over the Gulf of Mexico and Caribbean regions.

4. Discussion

4.1. Representativeness

How representative of the NAFC are the percent contributions discussed in section 3.6? The percent contributions of each source term along the SONEX flight paths are shown for experiment SGOL in column 1 of Table 5. The SONEX flight paths were not always within the NAFC (defined here to be 0°-70°W; 45°-60°N). The percent contributions for flights that were at least partially within the NAFC are shown in column 2. The percent contributions after averaging the model temporally over the length of the SONEX mission (October 13-November 12, 1997) and spatially over the NAFC are shown in columns 3-7. The average contributions at the "mean altitude" of the SONEX flights are shown in column 3, while the contributions at the sigma layers corresponding to approximately 353, 302, 258, and 221 hPa (a pressure range that included 84% of the measurements (see "weighting" row in Table 6) are shown in columns 4-7, respectively.

The relative importance of the stratospheric source to the upper tropospheric NO_y budget increases from 22 to 32% when the averaging area is changed from the SONEX flight paths to the NAFC. The rather large difference is not entirely surprising since regions where stratospheric

influence was expected to be large were often avoided if possible when planning SONEX flight paths. The relative role of the stratosphere is also very sensitive to the altitude of the flight paths. Model-calculated estimates of the relative importance of stratospheric NO_y increased from 23 to 53% when the sampling altitude was changed from 353 to 221 hPa.

The increase in stratospheric NO_y when considering the entire NAFC region is balanced by a fairly large decrease in the relative importance of lightning emissions (19 to 14%), a small decrease in the relative importance of fossil fuel/soil sources (44 to 42%), and a fairly sizeable (at least on a percentage basis (12 to 10%)) change in the relative importance of aircraft emissions. The decrease in the role of aircraft emissions is partially due to the fact that the goal of several of the flights was to characterize the air in the OTS after the traffic peaks. The relative importance of aircraft emissions increases slightly with decreasing pressure in the upper troposphere when averaging over the NAFC.

Therefore, conclusions about the NO_y budget in the NAFC based only on measurements from the SONEX flights will tend to underestimate the importance of the stratospheric source and overestimate the effect of lightning and to a smaller degree aircraft emissions. *Thompson et al.* [1999] came to a similar conclusion about the representativeness of the SONEX flight paths. They found by comparing 1992-1998 PDFs of potential vorticity that air parcels along the SONEX flight paths during 1997 were more subtropical and less stratospheric than the 1992-1998 average.

4.2. Performance of lightning algorithm

Price and Rind [1994b] evaluate an algorithm used to parameterize lightning emissions in the GISS (Goddard Institute for Space Studies) GCM by comparing latitudinal and diurnal

variations in model-calculated lightning flashes with measurements. We will compare model-calculated flash rates between 10°-60°N and 120°-60°W with NLDN/LRF flash rates from the same region that have been adjusted for detection efficiency. Our goal is to illustrate the uncertainties that remain in both the detection efficiency and the algorithm for parameterizing lightning emissions.

The cloud-to-ground flash rates used in these simulations were parameterized using November 1-9, 1997 GEOS-STRAT mass fluxes at 0.44 sigma between 10°-60°N and 120°-60°W. The fit was excellent when averaged over the entire region and time period (see Figure 2) with the model-calculated and NLDN-LRF flash rates equalling 199 and 201 flashes per day, respectively; however, the fit is not as good when the flash rates are binned by latitude (Figure 11a) . The algorithm overpredicts low latitude (10°-25°N) flashes by a factor of 1.75 while underpredicting mid-latitude flashes by ≈30%. The bias is probably caused by a combination of factors. 1) The GEOS-DAS overpredicts deep convection in the tropics and low latitudes and underpredicts deep convection at higher latitudes especially in the marine storm tracks *[Molod et al.*, 1996; *Allen et al.*, 1997]. 2) The detection efficiencies for the lightning flash rates outside the United States that are used to calculate lightning emissions are almost certainly too optimistic (see section 3.5). The error caused by overestimating the efficiencies increases with distance from the United States.

The "GEOS-STRAT" and NLDN/LRF flash rates as a function of time of day are plotted in Figure 11b. The algorithm overpredicts (relative to the adjusted NLDN/LRF flash rates) the flash rate during the afternoon (18UT) while underpredicting it during the morning (12UT). The bias is partially caused by our assumption that the detection efficiency is the same during the day

and at night. Results from a recent field study [*Cramer and Cummins*, 1998] indicate that the detection efficiency is much higher at night than during the day. The morning peak in the adjusted NLDN/LRF flash rates may exist because we have not adjusted for diurnal changes in detection efficiency. The bias is reduced but still remains when we limit our domain to grid points over the United States (not shown). This suggests that the bias may also be due to biases in deep convective activity in the GEOS-STRAT DAS. Specifically, it appears that the GEOS-STRAT DAS overestimates the intensity of deep convection during the afternoon and underestimates its intensity during the morning.

4.3. Loss by scavenging

The assumption that the removal of NO_y by scavenging/settling is a first order process is extremely crude and does not allow the conclusions drawn from this study to be as strong as we would like. Model calculations [*Rodhe*, 1983; *Giorgi and Chameides*, 1986] have shown that the wet-scavenging lifetime of tracers with predominantly surface sources is shorter than the lifetime of tracers with predominantly stratospheric sources. The difference in lifetimes results from the fact that wet scavenging is larger in regions of net upward motion than in regions of net downward motion. Therefore, tracers with a net upward flux (ie., tracers with predominantly surface sources) are preferentially scavenged.

The high-bias in the model is at least partially due to the first order algorithm used to parameterize wet scavenging in the SG-GCTM. A more realistic scavenging algorithm that accounts for first-order losses by rainout and washout in large-scale and convective precipitation events has been added to versions of the Goddard CTM (*M. Chin*, personal communication, 1998) and may be used in the future. The loss rate in this algorithm is computed based on the

algorithms of *Giorgi and Chameides* [1986] and *Balkanski et al.* [1993]. These algorithms require the vertical distribution of precipitation; a field that is not available from the GEOS-STRAT DAS. Because of this, the vertical distribution of precipitation is estimated by normalizing the specific humidity change due to condensation and evaporation by the surface precipitation rate.

A more realistic scavenging algorithm may not improve this simulation as much as hoped. Estimates of the November 1997 daily precipitation over eastern North America and the Atlantic from the GEOS-1 DAS and from the GPCP (Global Precipitation Climatology Project; *Huffman et al.*, 1997]) are shown in Figures 12a-b. The ratio of GEOS-1 DAS precipitation amounts to GPCP precipitation amounts is less than 0.4 over portions of the North Atlantic storm track and more than 2 over portions of the Caribbean (Figure 12c). These biases in the intensity of convection are consistent with earlier studies [*Allen et al.*, 1997] which showed that the intensity of deep convection in the GEOS-1 DAS is underestimated along the North Atlantic storm track and overestimated in the Caribbean.

Precipitation amounts during November 1997 (Figure 12b) along the North Atlantic storm track were larger than usual (Figure 12d). Therefore, wet scavenging during November 1997 is likely to have been larger than usual, and the mean lifetimes used in this simulation are likely to be too large during November. A sensitivity calculation was run with the uniform grid CTM where the upper tropospheric lifetimes were adjusted by multiplying by the ratio of the mean November GPCP precipitation to the November 1997 GPCP precipitation. The high-bias was reduced by a few percent.

5. Summary

The relative importance of various NO_x sources including lightning, aircraft, and surface emissions on upper tropospheric NO_y in the NAFC is illustrated as a first application of the SG-GCTM. Spatial variations in NO_y were well captured especially with the stretched-grid run; however, model-calculated concentrations were often too high in the upper troposphere. Aircraft emissions play a relatively minor role in the upper tropospheric NO_y budget averaged along SONEX flight paths (12%); however, the contribution of emissions is as large as ≈30% during portions of some flights.

Estimates of the relative importance of aircraft emissions on upper tropospheric NO_x and NO_y budgets differ widely. The estimate for NO_y obtained in this study (10-12%) is on the lower end of estimates cited in the introduction. Large differences exist because each investigator phrased the problem differently (in terms of the geographic region considered, the definition of the upper troposphere, the choice of NO_x or NO_y, the definition of the stratospheric contribution, etc.) and used a different set of tools (CTMs, meteorological fields, lightning algorithms, etc.) to answer it. However, regardless of how the question is phrased, estimates will continue to vary widely until uncertainties in stratosphere-troposphere exchange and in the parameterization of lightning NO_x emissions, deep convective mixing, and wet scavenging are reduced.

The lightning algorithm does a reasonably good job; however, the use of observed lightning emissions significantly improves the simulation on a few occasions, especially November 3, 1997. Uncertainties in the lightning algorithm remain large but will be reduced as lightning flash data become available for more time periods and for other areas. Errors will also be reduced when more accurate estimates of the detection efficiency and the ratio of the energy of intracloud to

cloud-to-ground flashes become available.

These calculations were performed using a stretched-grid CTM; however, the dynamical fields used to drive the model were obtained from a coarser uniform grid model. Future calculations will use driving fields from a stretched-grid data assimilation system. Over the next year, stretched-grid data are expected to be available for the SONEX (13 October to 12 November 1997), AEROCE (2 April to 3 May, 1996), PRE-STORM (June 1985), MAPS (April and October 1994), and INDOEX (15 February to 31 March 1999) periods. Stretched-grid simulations using dynamical fields from a stretched-grid DAS are necessary before the full value of stretched-grid CTM simulations can be determined.

Appendix

The mixing ratio change due to advection was calculated by modifying *Lin and Rood's* [1996, *LR96* hereafter) multidimensional and semi-Lagrangian extension of the PPM [*Colella and Woodward*, 1984; *Carpenter et al.*, 1996] for use on a non-uniform grid. The three-dimensional transport equation can be expressed symbolically as (equation 4.2 of *LR96*):

$$q^{n+1} = \{Q^n + F[q^n + 1/2g(q^n)] + G[q^n + 1/2f(q^n)] + H[q^n]\} / \pi^{n+1} \qquad \text{(A1)}$$

where q = mixing ratio, π = surface pressure, n = time step index, Q = πq = constituent density, F(G) = change of quantity in brackets due to flux-form transport from the east-west (north-south) direction, H = change of quantity in brackets due to flux-form transport from the vertical direction, f(g) = change of quantity in brackets due to advective-form transport from the east-west (north-south) direction. An equation for π is obtained by setting q=1 in (A1) and integrating from the top (σ =0) to the bottom (σ =1) of the vertical σ domain to obtain (equation 4.3 of *LR96*):

$$\pi^{n+1} = \pi^n + \int_0^1 (F[1] + G[1]) d\sigma \qquad \text{(A2)}$$

The f and g operators are needed to minimize operator splitting errors that arise because the east-west and north-south convergence terms are calculated sequentially. The f and g operators must be expressed in their advective form in order to ensure that the constituent continuity equation reduces to the continuity equation for a spatially uniform q field [*LR96*]. The operator splitting terms represented by f and g are of a higher order than their flux-form counterparts. Therefore, the splitting terms are calculated using first-order upwind differencing after defining the velocity field, surface pressure, and mixing ratio at box centers.

The change in the constituent density at grid point i due to "flux-form" east-west, north-south, or vertical transport can be expressed as (Equation 3.3 of *LR96*):

$$Q_i(n+1) = Q_i(n) + [F_{i-1/2}(n+1/2) - F_{i+1/2}(n+1/2)]/\Delta x_i \,, \qquad \text{(A3)}$$

where $F_{i-1/2}$ (equal to $u_{i-1/2}\Delta t\ \pi_{i-1/2}q_{i-1/2}$) and $F_{i+1/2}$ (equal to $u_{i+1/2}\Delta t\ \pi_{i+1/2}q_{i+1/2}$) are the time-averaged fluxes across the "left" and "right" edges of grid box i, respectively, and Δx_i is the width of grid box i. Values for the *u* and *v* components of the wind and π at the "left" edge of grid box i (i=i-½) are obtained by averaging the values at the centers of grid boxes i-1 and I (see Figure A1). Vertical velocities at the layer edges are calculated kinematically by integrating the continuity equation in the vertical from the model top where $\sigma = 0$ to the desired σ layer. The mixing ratios at the box edges ($q_{i-1/2}$ and $q_{i+1/2}$) are approximated using the PPM subject to the monotonicity constraints of *Colella and Woodward* [1984] in the horizontal and *LR96* in the vertical.

The approach of *LR96* is used to extend the scheme to long time steps (ie., time steps where the CFL condition is violated in the east-west or north-south directions). The constituent flux is divided into "integer" and "fractional" parts by dividing the Courant number ($C_{i-1/2}$) into

integer and fractional parts. Mathematically (equation 3.1 of *LR96*),

$$C_{i-1/2} = K_{i-1/2} + c_{i-1/2}, \tag{A4}$$

where $K_{i-1/2}$ is the integer part of $C_{i-1/2}$, and $c_{i-1/2}$, the fractional part. The fractional Courant number, $c_{i-1/2}$, is given by (equation 3.2 of *LR96*)

$$c_{i-1/2} = \mathrm{mod}(C_{i-1/2}, K_{i-1/2}) \tag{A5}$$

The expression for $C_{i-1/2}$ is more complicated than in *LR96* because Δx and Δy are not constant. Mathematically,

$$C_{i-1/2} = (i-1-ii) + dx_{ii} / \Delta x_{ii}, \qquad (u_{i-1/2} \geq 0)$$

$$C_{i-1/2} = (i-ii) + dx_{ii} / \Delta x_{ii}, \qquad (u_{i-1/2} < 0) \tag{A6}$$

The integer part (the term in parentheses) of $C_{i-1/2}$ can be interpreted as the number of complete grid boxes traveled by a parcel during Δt assuming a velocity of $u_{i-1/2}$. It equals zero when the CFL condition is not violated. The index of the grid box the parcel was located in at the beginning of the time step (the "departure" grid box) is given by ii. Mathematically, ii is determined by summing Δx_j until a value of j is found for which

$$\sum_{j=i-1}^{ii} \Delta x_j > |u_{i-1/2}| \Delta t, \quad j=i-1, i-2, \ldots, ii \qquad (u_{i-1/2} \geq 0)$$

$$\sum_{j=i}^{ii} \Delta x_j > |u_{i-1/2}| \Delta t, \quad j=i, \; i+1, \ldots, ii \qquad (u_{i-1/2} < 0) \tag{A7}$$

The fractional part of C can be interpreted as the fraction of the departure grid box the parcel encountered during Δt. Mathematically, dx_{ii} is given by

$$dx_{ii} = |u_{i-1/2}| \Delta t - \sum_{j=i-1}^{ii+1} \Delta x_j \qquad u_{i-1/2} \geq 0$$

$$dx_{ii} = |u_{i-½}|\,\Delta t - \sum_{j=I}^{ii-1} \Delta x_j \qquad u_{i-½} < 0 \tag{A8}$$

The calculation of the Courant number when the CFL condition is violated in the east-west direction is illustrated for the case where $u_{i-½} = 100$ m s^{-1}, $\Delta x_i = 100$ km, $\Delta x_{i-1} = 75$ km, $\Delta x_{i-2} = 50$ km, and $\Delta t = 1000$s in Figure A1. Solving (A7) for ii we obtain ii = i-2, solving (A8) for dx_{ii} we obtain $dx_{ii} = 25$ km, and solving (A5) for $C_{i-½}$, $K_{i-½}$, and $c_{i-½}$ we obtain 1.5, 1, and 0.5, respectively.

The fractional flux is solved for using the PPM as before; however, a different algorithm is needed to solve for the integer flux because the PPM is unstable for $|C| > 1$. The "integer" flux is calculated using a semi-Lagrangian approach. In this case, the constituent density at the box edges is assumed to be given by a weighted average of the constituent densities in all the boxes encountered during Δt. The contributions from the "integer" and "fractional" components of the flux can be combined to get an estimate for the constituent density at the box edges. This estimate is used to solve Equation (A3). Mathematically,

$$Q_{i-1/2}(n+1/2) = \left[\sum_{j=i-1}^{ii+1}(Q_j\,\Delta x_j) + Q_{ii}(n+1/2)\,dx_{ii}\right] \Big/ \left[\sum_{j=i-1}^{ii+1}(\Delta x_j) + dx_{ii}\right]$$

$$\text{for} \quad u_{i-½} \geq 0, \quad j=i-1,\ i-2,\ \ldots\ ,ii+1$$

$$Q_{i-1/2}(n+1/2) = \left[\sum_{j=i}^{ii-1}(Q_j\,\Delta x_j) + Q_{ii}(n+1/2)\,dx_{ii}\right] \Big/ \left[\sum_{j=i}^{ii-1}(\Delta x_j) + dx_{ii}\right]$$

$$\text{for} \quad u_{i-½} < 0, \quad j=i,\ i+1,\ \ldots\ ,ii-1 \tag{A9}$$

where Q_{ii} is calculated using the second-order PPM. The summation terms drop out for $|C| < 1$. The Δx_j and dx_{ii} terms in the numerator and denominator cancel if the grid is uniform.

Analogous expressions are used to calculate the change in constituent density due to north-

south transport. An additional complication arises for cross-polar flow when the CFL condition is violated in the north-south direction. In this case, in order to solve (A9), the constituent density is needed at fictitious grid points 180° (on the opposite side of the pole) from grid point i. Values at these fictitious grid points are obtained by interpolation using values at actual grid points on each side of the fictitious grid points. The need for fictitious grid points does not exist when the grid is uniform because in that case actual grid points exist that are 180° from grid point i.

Acknowledgements. This research was supported under a NASA/EOS Interdisciplinary Science Investigation (Grant NAG5-3678) and the NASA Atmospheric Effects of Aviation Project (Grants NAG5-7263 and NCC5-55).

References

Allen, D. J., R. B. Rood, A. M. Thompson, and R. D. Hudson, Three-dimensional radon-222 calculations using assimilated meteorological data and a convective mixing algorithm, *J. Geophys. Res.*, 101, 6871-6881, 1996a

Allen, D. J., P. Kasibhatla, A. M. Thompson, R. B. Rood, B. G. Doddridge, K. E. Pickering, R. D. Hudson, and S.-J. Lin, Transport-induced interannual variability of carbon monoxide determined using a chemistry and transport model, *J. Geophys. Res*, 101, 28,655-28,669, 1996b.

Allen, D. J., K. E. Pickering, and A. Molod, An evaluation of deep convective mixing in the Goddard Chemical Transport Model using International Satellite Cloud Climatology Project cloud parameters, *J. Geophys. Res.*, 102, 25,467-25,476, 1997.

Baker, M. B., H. J. Christian, and J. Latham, A computational study of the relationships linking lightning frequency and other thundercloud parameters, *Q. J. R. Meteorol. Soc.*, 121, 1525-1548, 1995.

Balkanski, Y. J., D. J. Jacob, G. M. Gardner, W. C. Graustein, and K. K. Turekian, Transport and residence times of tropospheric aerosols inferred from a global three-dimensional simulation of ^{210}Pb, *J. Geophys. Res.*, 98, 20,573-20,586, 1993.

Baugchum, S. L., Subsonic aircraft emissions inventories, in *Atmospheric Effects of Aviation: First Report of the Subsonic Assessment Project*, NASA Reference Publication 1385, 15-29, 1996.

Benkovitz, C. M., T. Scholtz, J. Pacyna, L. Tarrassn, J. Dignon, E. Voldner, P. A. Spiro, J. A. Logan, and T. E. Graedel, Global inventories of anthropogenic emissions of SO_2 and NO_x, *J. Geophys. Res.*, 101, 29,239-29,253, 1996.

Bloom, S. C., L. L. Takacs, A. M. DaSilva, and D. Ledvine, Data assimilation using incremental analysis updates, *Mon. Weather Rev.*, 124, 1256-1271, 1996.

Boeing Commercial Airplane Group, *1996 Current Market Outlook*, 1996.

Brasseur, G. B., J.-F. Müller, and C. Granier, Atmospheric impact of NO_x emissions by subsonic aircraft: A three-dimensional model study, *J. Geophys. Res.*, 101, 1423-1428, 1996.

Carpenter, R. L., Jr., K. K. Drogemeier, P. R. Woodward, and C. E. Hane, Application of the piecewise parabolic method to meteorological modeling, *Mon. Weather. Rev.*, 118, 586-612, 1990.

Chatfield, R. B., and A. C. Delany, Convection links biomass burning to increased tropical ozone: However, models will tend to overpredict O_3, *J. Geophys. Res.*, 95, 18,473-18,488, 1990.

Chin, M., R. B. Rood, D. J. Allen, M. O. Andreae, A. M. Thompson, S.-J. Lin, R. M. Atlas, and J. V. Ardizzone, Processes controlling dimethylsulfide over the ocean: Case studies using a 3-D model driven by assimilated meteorological fields, *J. Geophys. Res.*, 103, 8341-8353, 1998.

Colella, P., and P. R. Woodward, The piecewise parabolic method (PPM) for gas-dynamical simulations, *J. Comput. Phys.*, 54, 174-201, 1984.

Cramer, J. A., and K. L. Cummins, Long Range and Trans-oceanic Lightning Detection, Paper presented at the 1998 International Lightning Detection Conference, Tucson, AZ, Nov 17-18, 1998.

Davis, D., et al., A case study of SONEX flight 10 in the North Atlantic, I: Sources and time evolution of NO_x and HO_x chemistries, *J. Geophys. Res.*, this issue.

Dignon, J., and J. E. Penner, Biomass burning: A source of nitrogen oxides to the atmosphere, in *Global Biomass Burning: Atmospheric, Climatic, and Biospheric Implications*, edited by J. S. Levine, pp. 370-375, MIT Press, Cambridge, Mass., 1991.

Douglass Aircraft Company, *Outlook for Commercial Aircraft, 1994-2013*, 1995.

Douglass, A. R., and S. R. Kawa, Contrast between 1992 and 1997 high latitude spring HALOE obervations of lower stratospheric HCl, submitted, *J. Geophys. Res.*, 1999.

Douglass, A. R., R. B. Rood, S. R. Kawa, and D. J. Allen, A three-dimensional simulation of the evolution of the middle latitude winter ozone in the middle stratosphere, *J. Geophys. Res.*, 102, 19,217-19,232, 1997.

Ertel, H., Ein neuer hydrodynamischer Wirbelsatz, *Meteorol. Z.*, 59, 271-281, 1942.

Flatøy, F., and Ø. Hov, Three-dimensional model studies of the effect of NO_x emissions from aircraft on ozone in the upper troposphere over Europe and the North Atlantic, *J. Geophys. Res.*, 101, 1401-1422, 1996.

Fox-Rabinovitz, M., G. Stenchikov, M. Suarez, and L. Takacs, A finite-difference GCM dynamical core with a variable resolution stretched grid, *Mon. Weather Rev.*, 125, 2943-2968, 1997.

Fox-Rabinovitz, M., G. Stenchikov, M. Suarez, L. Takacs, and R. Govindaraju, A uniform and variable resolution stretched grid GCM dynamical core with a real orography, submitted, *Mon. Weather Rev.*, 1999.

Friedl, R. R. et al. (Eds.), Atmospheric effects of subsonic aircraft: Interim assessment report of the Advanced Subsonic Technology Program, *NASA Ref. Publ.*, 1400, 168 pp., Nat. Aeronaut. And Space Admin., Greenbelt, Md., 1997.

Gallardo, L., and V. Cooray, Could cloud-to-cloud discharges be as effective as cloud-to-ground discharges in producing NO_x?, *Tellus*, 48B, 641-651, 1996.

Gallardo, L., and H. Rodhe, Oxidized nitrogen in the remote Pacific: The role of electrical discharges over the oceans, *J. Atmos. Chem.*, 26, 147-168, 1997.

Giorgi, F., and W. L. Chameides, Rainout lifetimes of highly soluble aerosols and gases as inferred from simulations with a general circulation model, *J. Geophys. Res.*, 91, 14,367-14,376, 1986.

Hao, W. M., and M.-H. Liu, Spatial and temporal distribution of tropical biomass burning, *Global Biogeochem. Cycles*, 8, 495-503, 1994.

Hauglustaine, D. A., C. Granier, G. P. Brasseur, and G. Mégie, Impact of present aircraft emissions of nitrogen oxides on tropospheric ozone and climate forcing, *Geophys. Res. Lett.*, 21, 2031-2034, 1994.

Huffman, G. J., R. F. Adler, P. Arkin, A. Chang, R. Ferraro, A. Gruber, J. Janowiak, A. McNab, B. Rudolf, and U. Schneider, The Global Precipitation Climatology Project (GPCP) combined precipitation dataset, *Bull. Am. Meteorol. Soc.*, 78, 5-20, 1997.

Jackman, C. H., E. L. Fleming, S. Chandra, D. B. Considine, and J. E. Rosenfield, Past, present, and future modeled ozone trends with comparisons to observed trends, *J. Geophys. Res.*, 101, 28,753-28,767, 1996.

Jeker, D., H. Wenli, D. Brunner, J. Staehelin, K. E. Pickering, A. M. Thompson, H. B. Selkirk, L. Pfister, and L. Jaegle, Nitrogen oxides and ozone from B-747 measurements during POLINAT-2/SONEX: Overview and case studies on convection, *J. Geophys. Res.*, this issue.

Kasibhatla, P., NO_y from sub-sonic aircraft emissions: A global three dimensional model study, *Geophys. Res. Lett.*, 20, 1707-1710, 1993.

Lamarque, J.-F., G. P. Brasseur, P. G. Hess, and J.-F. Müller, Three-dimensional study of the relative contributions of the different nitrogen sources in the troposphere, *J. Geophys. Res.*, 101, 22,955-22,968, 1996.

Lawrence, M. G., and P. J. Crutzen, The impact of cloud particle gravitational setting on soluble trace gas distributions, *Tellus*, 50B, 263-289, 1998.

Levy, H. II., W. J. Moxim, and P. S. Kasibhatla, A global three-dimensional time-dependent lightning source of tropospheric NO_x, *J. Geophys. Res.*, 101, 22,911-22,922, 1996.

Lin, S.-J., and R. B. Rood, Multidimensional flux form semi-Lagrangian transport schemes, *Mon. Weather Rev.*, 124, 2046-2070, 1996.

Liu, S. C., M. Trainer, F. C. Fehsenfeld, D. D. Parrish, E. J. Williams, D. W. Fahey, G. Hübler, and P. C. Murphy, Ozone production in the rural troposphere and the implications for regional and global ozone distributions, *J. Geophys. Res.*, 92, 4191-4207, 1987.

Logan, J. A., M. J. Prather, S. C. Wofsy, and M. B. McElroy, Tropospheric chemistry: A global perspective, *J. Geophys. Res.*, 86, 7210-7254, 1981.

MacGorman, D. R., and W. D. Rust, *The Electrical Nature of Storms*, 422 pp., Oxford Univ. Press, New York, 1998.

Meijer, E. W., P. F. J. van Velthoven, A. M. Thompson, L. Pfister, H. Schlager, P. Schulte, and H. Kelder, Model calculations of the impact of air traffic, lightning, and surface emissions, compared with measurements, In press, *J. Geophys. Res.*, 1999.

Molod, A., H. M. Helfand, and L. L. Takacs, The climatology of parameterized physical processes in the GEOS-1 GCM and their impact on the GEOS-1 data assimilation system, *J. Clim.*, 9, 764-785, 1996.

Ozone Transport Assessment Group (1997), OTAG Technical Support Document, U.S. Environmental Protection Agency, http://www.eps.gov/otag, 1997a.

Ozone Transport Assessment Group (1997), OTAG Clearinghouse, MCNC Supercomputing Center, http://envpro.ncsc.org/OTAGDC, 1997b.

Pfister, L., H. B. Selkirk, et al., Estimates of convection based on satellite imagery, *J. Geophys. Res.*, this issue.

Pickering, K. E., Y. Wang, W.-K. Tao, C. Price, and J.-F. Muller, Vertical distributions of

lightning NO_x for use in regional and global chemical transport models, *J. Geophys. Res.*, 103, 31,203-31,216, 1998.

Pickering, K. E., A. M. Thompson, L. Pfister, T. L. Kucsera, Y. Kondo, G. W. Sachse, B. E. Anderson, and D. R. Blake, Comparison and interpretation of chemical measurements from two SONEX flights over the Canadian maritimes: Lightning, convection, and aircraft signatures, *J. Geophys. Res.*, this issue.

Price, C., and D. Rind, A simple lightning parameterization for calculating global lightning distributions, *J. Geophys. Res.*, 97, 9919-9933, 1992.

Price, C., and D. Rind, What determines the cloud-to-ground lightning fraction in thunderstorms?, *Geophys. Res. Lett.*, 20, 463-466, 1993.

Price, C., and D. Rind, Possible implications of global climate change on global lightning distributions and forecasts, *J. Geophys. Res.*, 99, 10,823-10,831, 1994a.

Price, C., and D. Rind, Modeling global lightning distributions in a general circulation model, *Mon. Wea. Rev.*, 1930-1939, 1994b.

Price, C., J. Penner, and M. Prather, NO_x from lightning, 1. Global distribution based on lightning physics, *J. Geophys. Res.*, 5929-5941, 1997a.

Price, C., J. Penner, and M. Prather, NO_x from lightning, 2. Constraints from the global atmospheric electric circuit, *J. Geophys. Res.*, 5943-5951, 1997b.

Rodhe, H., Precipitation scavenging and tropospheric mixing, in *Precipitation Scavenging, Dry Deposition, and Resuspension*, edited by H. R. Pruppacher, R. B. Semonin, and W. G. N. Slinn, pp. 719-729, Elsevier, New York, 1983.

Schlager, H., P. Konopka, P. Schulte, U. Schumann, H. Ziereis, F. Arnold, M. Klemm, D. E. Hagen, P. D. Whitefield, and J. Ovarlez, In situ observations of air traffic emission signatures in the North Atlantic flight corridor, *J. Geophys. Res.*, 102, 10,739-10,750, 1997.

Schubert, S. D., R. B. Rood, and J. Pfaendtner, An assimilated data set for earth science applications, *Bull. Am. Meteorol. Soc.*, 74, 2331-2342, 1993.

Singh, H. B., A. M. Thompson, and H. Schlager, 1997 SONEX Airborne Mission Overview and Accomplishments, submitted, *Geophys. Res. Lett.*, 1999.

Snow, J. A., B. G. Heikes, I. Simpson, D. R. Blake, H. B. Selkirk, H. E. Fuelberg, A. M. Thompson, N. Blake, and J. Hannan, A comparison of convective tracers during SONEX, *J. Geophys. Res.*, this issue.

Thompson, A. M., L. C. Sparling, Y. Kondo, B. E. Anderson, G. L. Gregory, and G. W. Sachse, Aircraft NO_x had no unique fingerprint on SONEX but lightning was the most likely NO_x source, submitted, *Geophys. Res. Lett.*, 1999.

Thompson, A. M., L. Pfister, T. L. Kucsera, L. R. Lait, H. B. Selkirk, K. E. Pickering, Y. Kondo, and G. Gregory, The Goddard/Ames Meteorological Support and Modeling System during SONEX: Evaluation of analyses and trajectory-based model products with tracer data, *J. Geophys. Res.*, this issue.

Van Leer, B., Toward the ultimate conservative difference scheme. Part V: A second order Godunov's method, *J. Comput. Phys.*, 32, 101-136, 1979.

Wacker, R. S., and R. E. Orville, Changes in measured flash count and return stroke peak current after the 1994 U. S. National Lightning Detection Network upgrade, 1, Observations, *J. Geophys. Res.*, 104, 2151-2158, 1999.

Wang, Y.-J., A. W. DeSilva, G. C. Goldenbaum, and R. Dickerson, Nitric oxide production by simulated lightning: Dependence on current, energy, and pressure, *J. Geophys. Res.*, 103, 19,149-19,159, 1998.

Wang, Y., J., D. J. Jacob, and J. A. Logan, Global simulation of tropospheric O_3-NO_x-hydrocarbon chemistry, 1, Model formulation, *J. Geophys. Res.*, 103, 10,713-10,725, 1998.

Williams, E. R., Schumann resonance: A global tropical thermometer, *Science*, 256, 1184-1187, 1992.

Yienger, J., and H. Levy II, Empirical model of global soil-biogenic NO_x emissions, J. *Geophys. Res.*, 100, 11,447-11,464, 1995.

Zel'dovich, Y. B., and Y. P. Raizer, *Physics of Shock Waves and High-Temperature Hydronamic Phenomena*, 445 pp., Academic, San Diego, Calif., 1966.

Figure captions:

1. Horizontal grid used for SONEX NO_y stretched-grid simulation. Grid spacing is 0.94°(0.75°) in the east-west (north-south) direction in the high resolution region (100° to 50°W, 25°-50°N) and stretches to 2.5°(2.0°) in the east-west (north-south) direction on the opposite side of the globe. Every second grid point is shown with a "+". The stretched-grid has 248(170) points in the east-west (north-south) direction.

2. NLDN/LRF Flash rate (flashes in 2.5° x 2.0° grid box min^{-1}) as a function of GEOS-STRAT mass flux (kg min^{-1} m^2) at 0.44 sigma. Sorted flash rates and mass fluxes are shown by a "*". Fourth order fit to sorted data is shown with a line. Fit obtained using 10° to 60°N, 120° to 60°W data from November 1-9, 1997.

3. SONEX flight tracks for October 23 (SONEX flight 7), October 28 (SONEX Flight 9), October 29 (SONEX Flight 10), November 3 (SONEX Flight 12), and November 9 (SONEX Flight 14). The October 28th and November 9th paths are drawn with a thinner line to separate them from the October 23rd and November 3rd paths, respectively.

4. Model-calculated versus measured NO_y (pptv) on October 23, 1997. NO_y (pressure) data after averaging over 60 s are shown by asterisks (a line). Model-calculated NO_y is shown for the grid volume containing the measurement. The value for each 60-s period is obtained by linearly interpolating model output that is available at 0, 6, 12, and 18 UT. Shading is used to show the model-calculated contribution from each source term. The total shaded region gives the contribution from all source terms. Time periods where data are missing are unshaded. (a) Model output from experiment UGOL. (b) Model output from experiment SGOL.

5. Same as Figure 4 but for October 28, 1997. (a) Model output from experiment SGPL. (b) Model output from experiment UGOL.

6. Same as Figure 4 but for October 29, 1997. (a) Model output from experiment SGPL. (b) Model output from experiment UGOL.

7. Model-calculated NO_y (ppbv) from lightning as a function of longitude and latitude. Model output from experiment SGOL is shown after interpolating onto the 250 hPa surface. (a) 12 UT October 26, 1997; (b) 12 UT October 27, 1997; (c) 12 UT October 28, 1997; and (d) 12 UT October 29, 1997. The aircraft flight track on October 29 is shown with a dark line.

8. Same as Figure 4 but for November 3, 1997. (a) Model output from experiment UGOL. (b) Model output from experiment SGOL.

9. Same as Figure 4 but for November 9, 1997. Model output from SGPL.

10. Model-calculated contribution to total NO_y from each source term (experiment SGPL) on each flight date. Values obtained by averaging contributions calculated for each 60-s period (see Figure 4 discussion). Total contribution for the SONEX mission obtained by averaging the contributions

from each flight. (a) Contribution from each source term in pptv (b) Contribution from each source term in percent.

11. Mean November 1-9, 1997 cloud-to-ground flash rates (total flashes in a six hour period) for 120° to 60W° and 10° to 60°N as a function of latitude (a) and time of day (b). NLDN/LRF flash rates after adjusting for efficiency using the method described in section 2.2.2 are shown with light bars. Model-calculated flash rates are shown with dark bars.

12. The daily precipitation rate (mm/day) for November 1997 from the GEOS-1 STRAT DAS (a) and from the GPCP Version 1a Combined measurements (b). The ratio of (a)/(b) is shown in c. The unshaded region is where the ratio is between 0.7 and 1.3. The two darkest regions are where the ratio is less than 0.4 (the darkest region) and between 0.4 and 0.7. The two lightest regions are where the ratio is greater than 1.3 but less than 2.0 and where it is greater than 2.0 (the lightest region). The mean (1987-1997) November daily precipitation rate from the GPCP is shown in d.

Table 1. Sigma (σ) layers used for the SONEX NO_y simulation. Sigma is defined as follows: $\sigma = (p-p_{top})/(p_{sfc}-p_{top})$, where p is the pressure at the bottom edge or center of model layer K, p_{top} is the pressure at the model top (1 hPa), and p_{sfc} is the surface pressure.

K	$\sigma_{bot\ edge}$	σ_{center}	K	$\sigma_{bot\ edge}$	σ_{center}
1	1.000	0.994	14	0.278	0.258
2	0.988	0.972	15	0.238	0.221
3	0.955	0.930	16	0.203	0.188
4	0.906	0.876	17	0.172	0.158
5	0.846	0.813	18	0.145	0.133
6	0.780	0.746	19	0.122	0.112
7	0.711	0.675	20	0.103	0.095
8	0.640	0.605	21	0.086	0.080
9	0.571	0.537	22	0.073	0.067
10	0.504	0.472	23	0.062	0.057
11	0.440	0.410	24	0.052	0.045
12	0.380	0.353	25	0.038	0.029
13	0.325	0.302	26	0.020	0.010

Table 2. Percent of daily aircraft NO emissions within the OTS of the NAFC that are assumed to occur during each hour as a function of longitude.

Time (UT)	00.5	01.5	02.5	03.5	04.5	05.5	06.5	07.5	08.5	09.5	10.5	11.5
10°-23°W	0.4	0.4	0.4	4.0	4.0	12.0	12.0	12.0	4.0	4.0	4.0	6.0
23°-35°W	0.4	0.4	4.0	6.0	12.0	12.0	6.0	4.0	0.4	0.4	0.4	4.0
35°-48°W	4.0	4.0	12.0	12.0	12.0	4.0	4.0	0.4	0.4	0.4	0.4	0.4
48°-60°W	6.0	12.0	12.0	6.0	4.0	0.4	0.4	0.4	0.4	0.4	0.4	0.4

Time (UT)	12.5	13.5	14.5	15.5	16.5	17.5	18.5	19.5	20.5	21.5	22.5	23.5
10°-23°W	12.0	12.0	6.0	4.0	0.4	0.4	0.4	0.4	0.4	0.4	0.4	0.4
23°-35°W	4.0	12.0	12.0	12.0	4.0	4.0	0.4	0.4	0.4	0.4	0.4	0.4
35°-48°W	0.4	4.0	6.0	12.0	12.0	6.0	4.0	0.4	0.4	0.4	0.4	0.4
48°-60°W	0.4	0.4	4.0	4.0	12.0	12.0	12.0	4.0	4.0	0.4	0.4	4.0

Table 3. The NO_y lifetime for grid points in the boundary layer is assumed to equal 1.0 days over land, 2.5 days over water, and 4.0 days over ice. The NO_y lifetime (days) as a function of pressure (hPa) and underlying surface (land, water, or ice) for tropospheric grid points that are not in the boundary layer is determined by interpolating from the values shown below. The lifetime at grid points above the tropopause is assumed to be infinite. The final column ($\tau_{ice}/\tau_{no\ ice}$) is the ratio between the NO_y lifetime with ice particle scavenging and settling and the lifetime without those processes.

Pressure	Land	Water	Ice	$\tau_{ice}/\tau_{no\ ice}$
1000	1.00	2.50	4.00	1.00
800	3.00	3.75	4.50	1.00
600	5.00	5.00	5.00	1.00
500	7.40	7.40	7.40	0.74
400	13.86	13.86	13.86	0.77
300	30.40	30.40	30.40	0.80
200	41.65	41.65	41.65	0.85
100	54.00	54.00	54.00	0.90

Table 4. Mean NO_y production (Tg N yr^{-1}) from each source for October 1- November 14, 1997

Fossil fuel/soil	24.90
Lightning	3.56
Biomass burning	15.75
Aircraft	0.50
N_2O dissociation	0.84

Table 5. Percent contribution of each source term from experiment SGOL. The average of the percent contributions from each of the 14 flights is shown in column 1 ($SONEX_{ALL}$). The average of the percent contributions from the 12 flights at least partially within the NAFC (October 29 and November 12 are excluded) is shown in column 2 ($SONEX_{NAFC}$). Only measurements within the NAFC are used to calculate the percent contributions in column 2. The average of percent contributions from the model within the entire NAFC is shown in column 3. The percent shown in column three was obtained by summing the contributions in each layer after weighting each layer by the percent of the SONEX measurements in the NAFC that were taken in that layer. The average of the percent contributions for the 0.353, 0.302, 0.259, and 0.221 σ layers are shown in columns 4-7. The weighting given to each sigma layer when calculating the value in column 3 is shown in the "Weighting" row.

Region	$SONEX_{ALL}$	$SONEX_{NAFC}$	NAFC	
Fossil/soil	40	44	42	
Lightning	20	19	14	
Biomass	3	3	2	
Aircraft	11	12	10	
Stratosphere	26	22	32	
Weighting	NA	NA	NA	
Sigma layer	0.353	0.302	0.259	0.221
Fossil/soil	50	41	30	22
Lightning	16	15	14	12
Biomass	2	2	2	2
Aircraft	9	11	12	12
Stratosphere	23	31	42	53
Weighting	0.24	0.19	0.29	0.12

Stretch grid 248 longitudes 170 latitudes

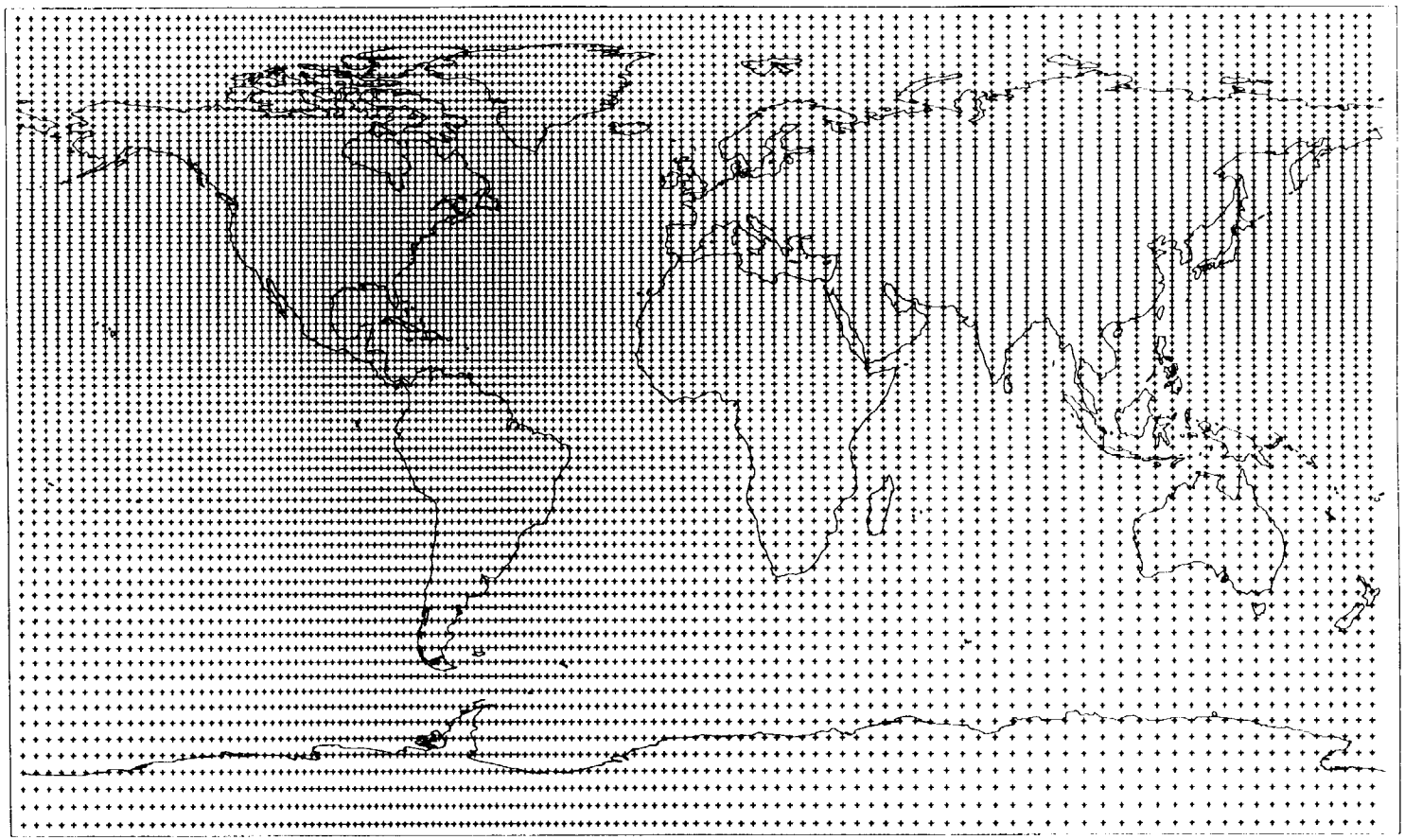

[0.94−2.50]E−W [0.75−2.00]N−S (Every 2nd pt shown)

High Resolution Area [−100.0W to −50.0W] [25.0N to 55.0N]

Figure 1

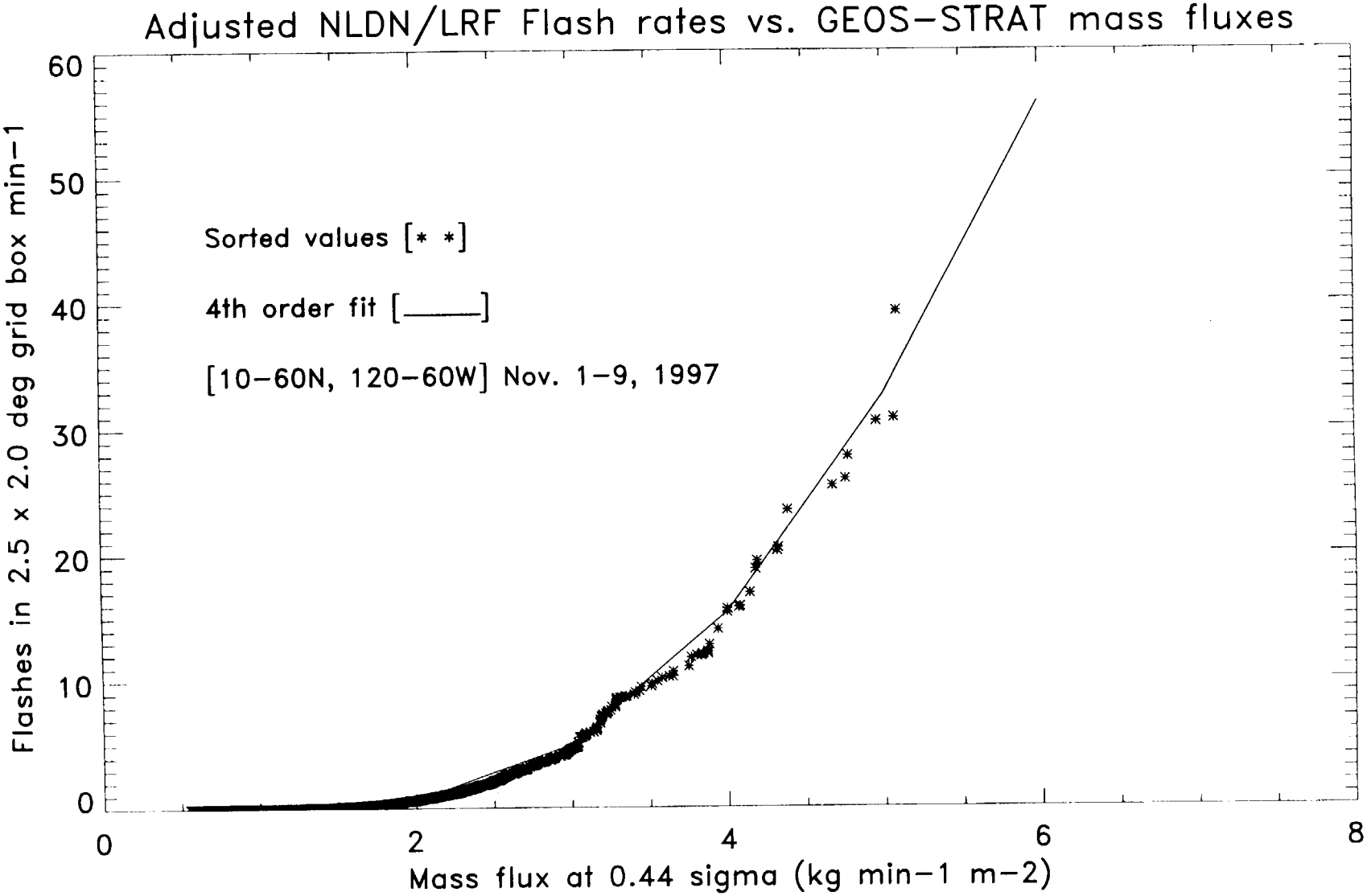
Adjusted NLDN/LRF Flash rates vs. GEOS-STRAT mass fluxes
Sorted values [* *]
4th order fit [_____]
[10-60N, 120-60W] Nov. 1-9, 1997
Flashes in 2.5 x 2.0 deg grid box min-1
Mass flux at 0.44 sigma (kg min-1 m-2)
0
10
20
30
40
50
60
0
2
4
6
8

Figure 2

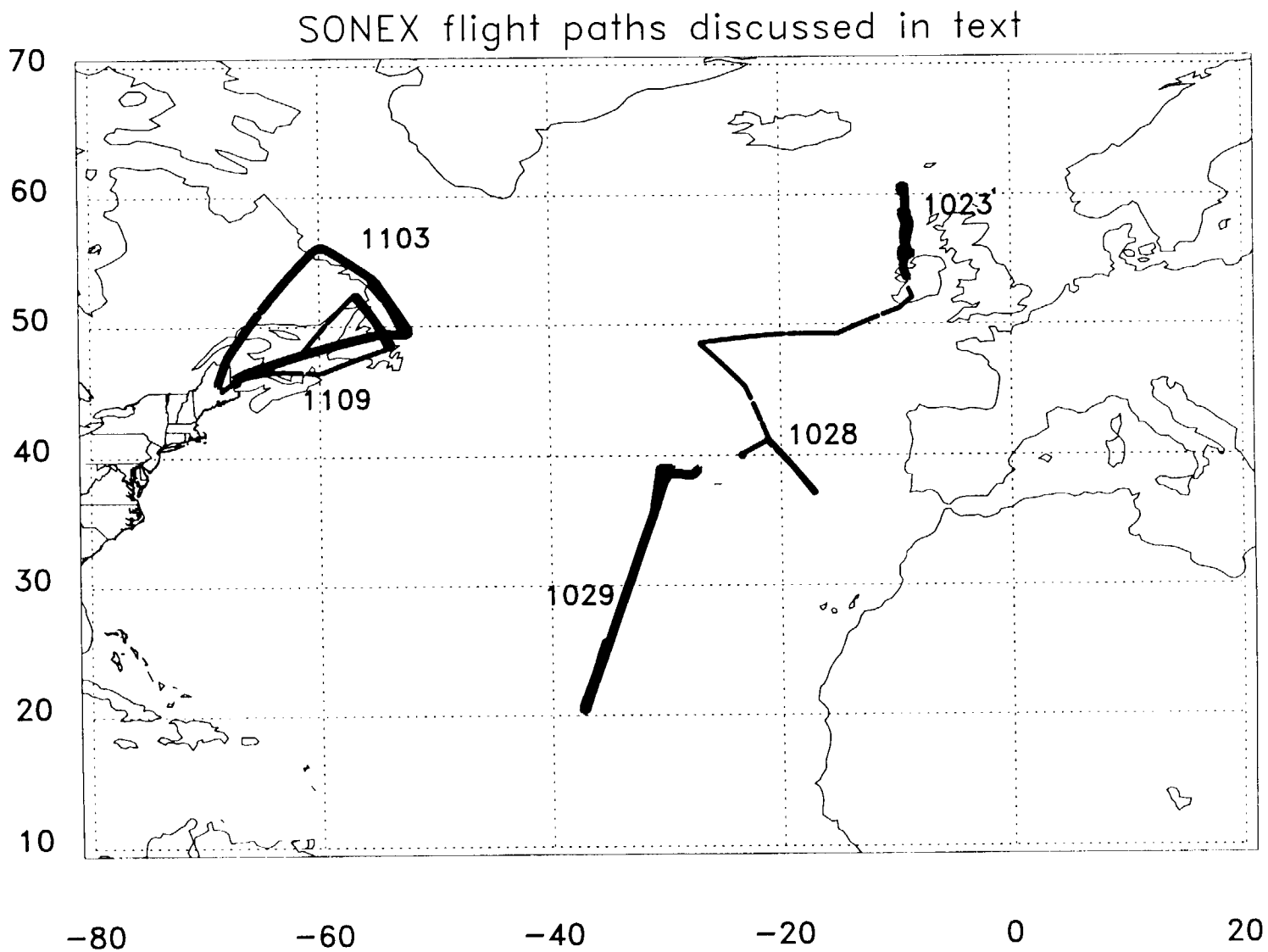
SONEX flight paths discussed in text
70
60
50
40
30
20
10
−80
−60
−40
−20
0
20
1103
1109
1023
1028
1029

Figure 3

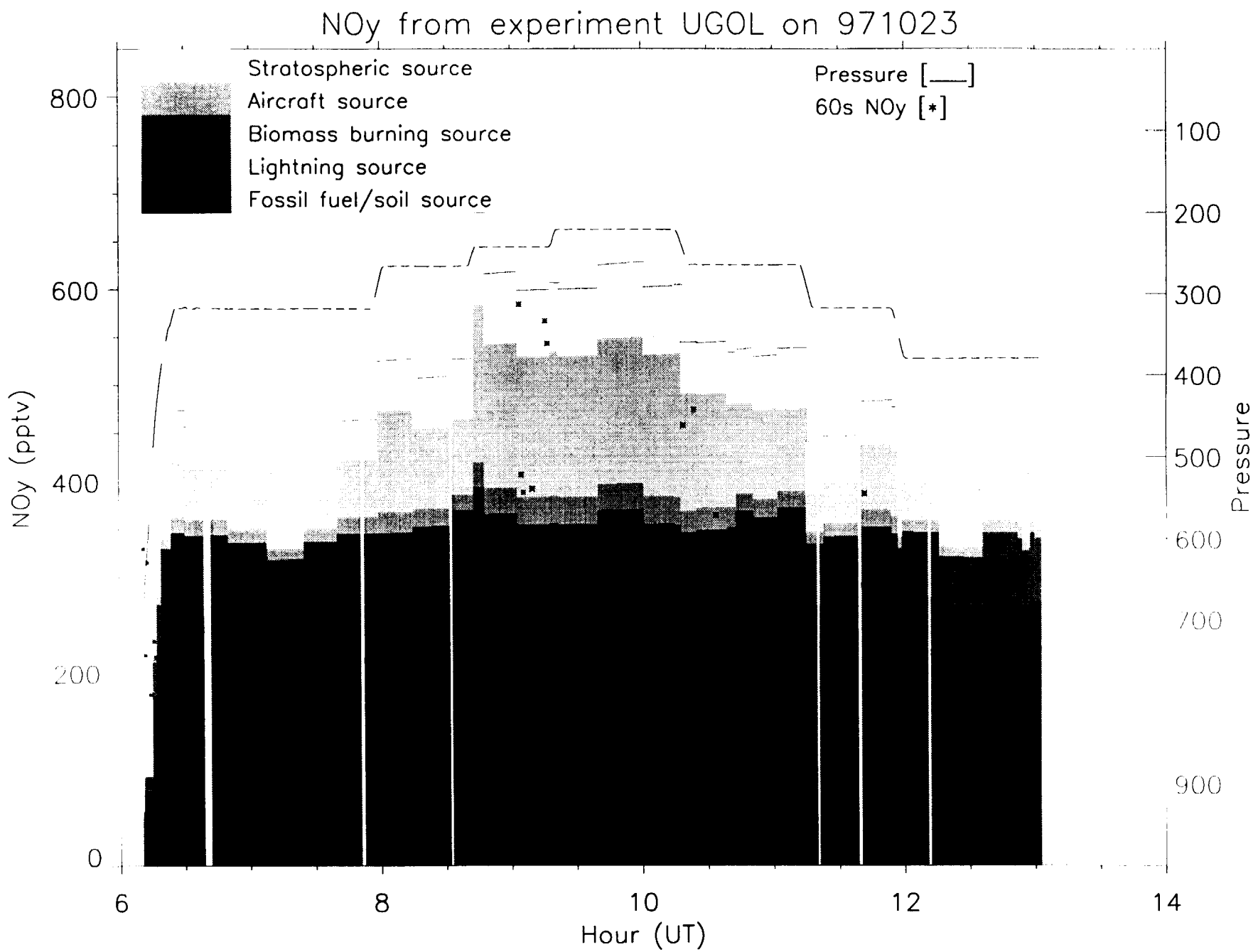
NOy from experiment UGOL on 971023
Stratospheric source
Aircraft source
Biomass burning source
Lightning source
Fossil fuel/soil source
Pressure [___]
60s NOy [*]
NOy (pptv)
800
600
400
200
0
6
8
10
12
14
Hour (UT)
100
200
300
400
500
600
700
900
Pressure

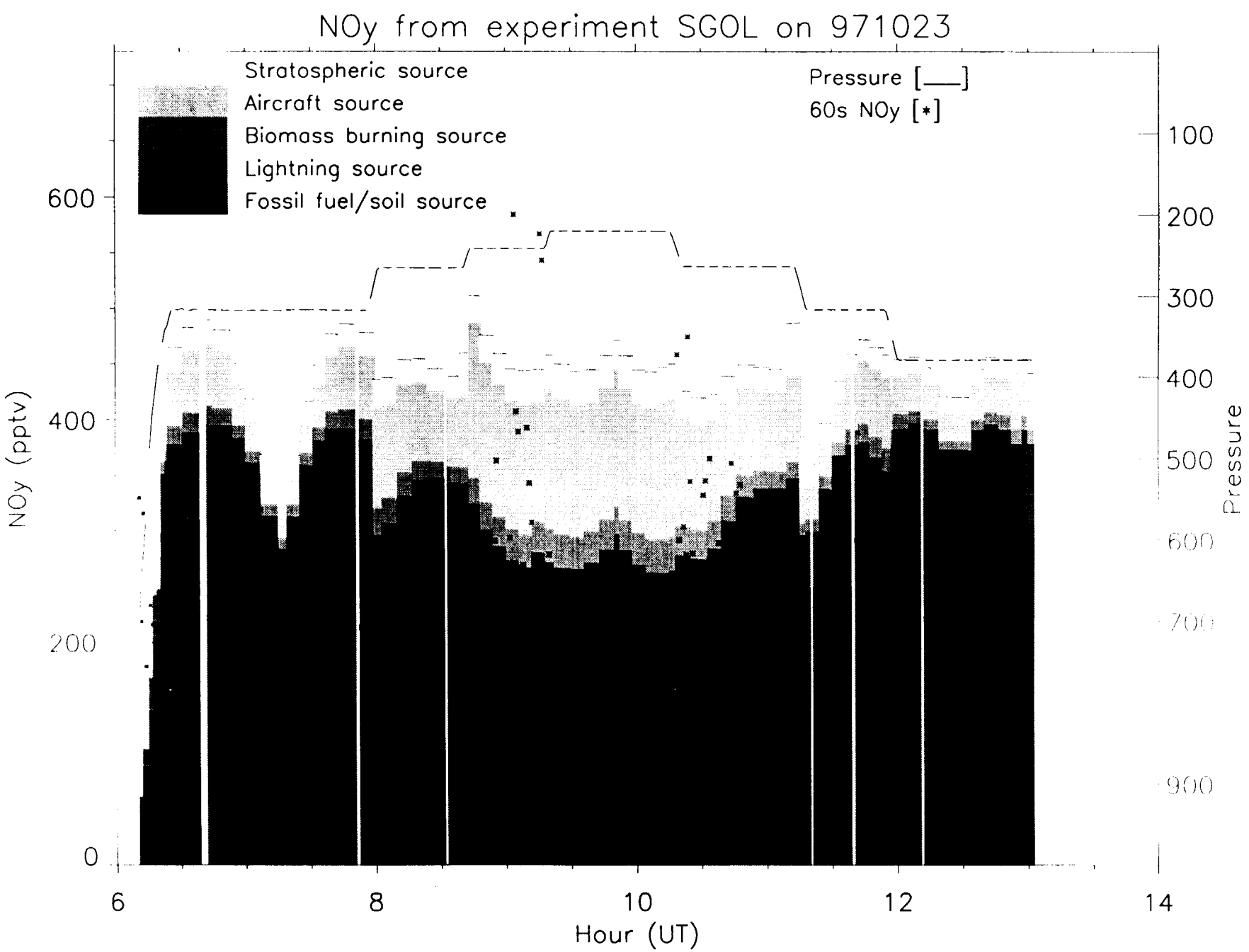
NOy from experiment SGOL on 971023
Stratospheric source
Aircraft source
Biomass burning source
Lightning source
Fossil fuel/soil source
Pressure [___]
60s NOy [*]
NOy (pptv)
0
200
400
600
6
8
10
12
14
Hour (UT)
100
200
300
400
500
600
700
900
Pressure

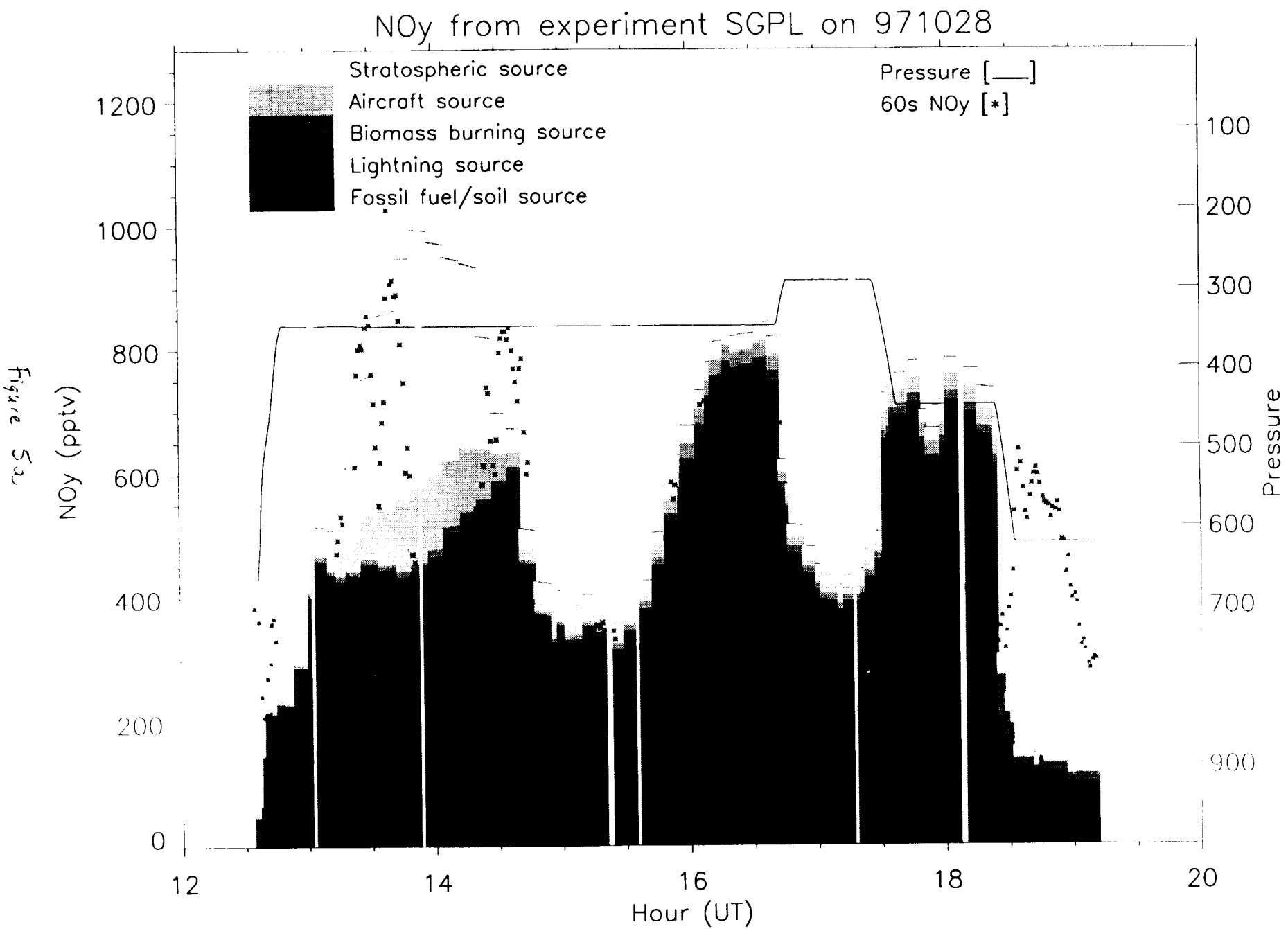
NOy from experiment SGPL on 971028
Stratospheric source
Aircraft source
Biomass burning source
Lightning source
Fossil fuel/soil source
Pressure [___]
60s NOy [*]
NOy (pptv)
Pressure
Hour (UT)
0
200
400
600
800
1000
1200
100
200
300
400
500
600
700
900
12
14
16
18
20

Figure 5a

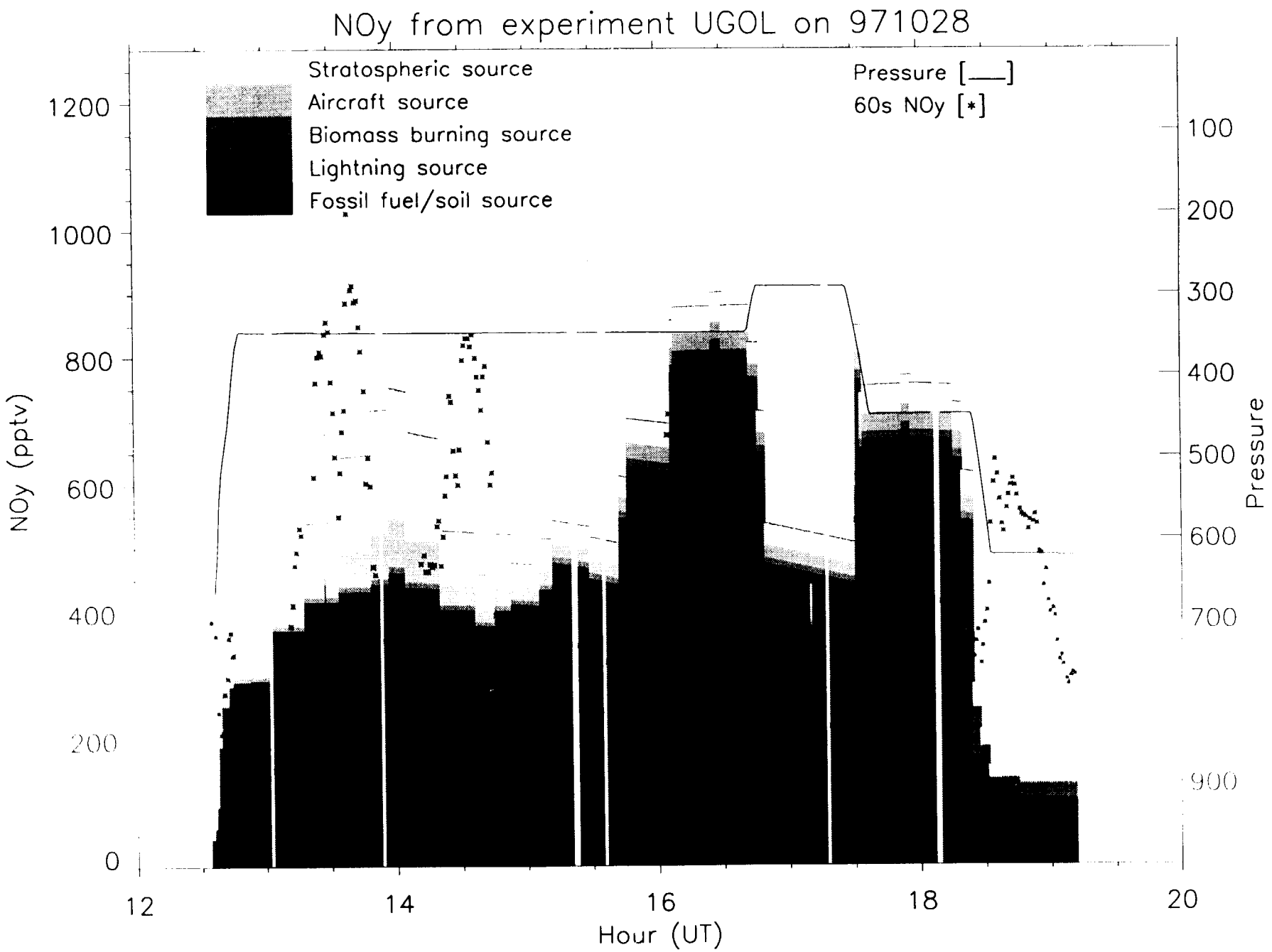
NOy from experiment UGOL on 971028
Stratospheric source
Aircraft source
Biomass burning source
Lightning source
Fossil fuel/soil source
Pressure [___]
60s NOy [*]
NOy (pptv)
Pressure
Hour (UT)
0
200
400
600
800
1000
1200
100
200
300
400
500
600
700
900
12
14
16
18
20

Figure 5a

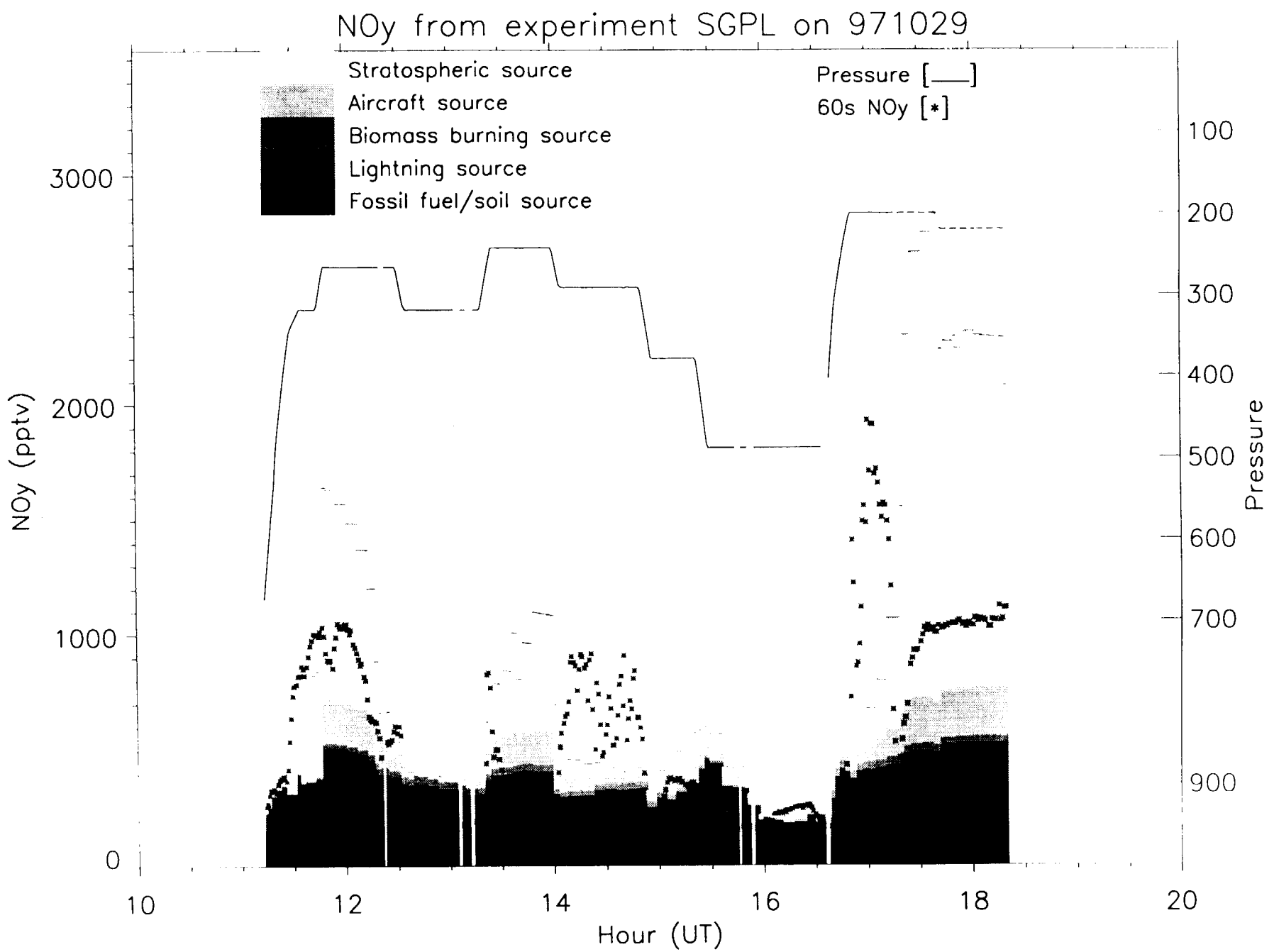
NOy from experiment SGPL on 971029
Stratospheric source
Aircraft source
Biomass burning source
Lightning source
Fossil fuel/soil source
Pressure [___]
60s NOy [*]
NOy (pptv)
Pressure
Hour (UT)
0
1000
2000
3000
100
200
300
400
500
600
700
900
10
12
14
16
18
20

Figure 6a

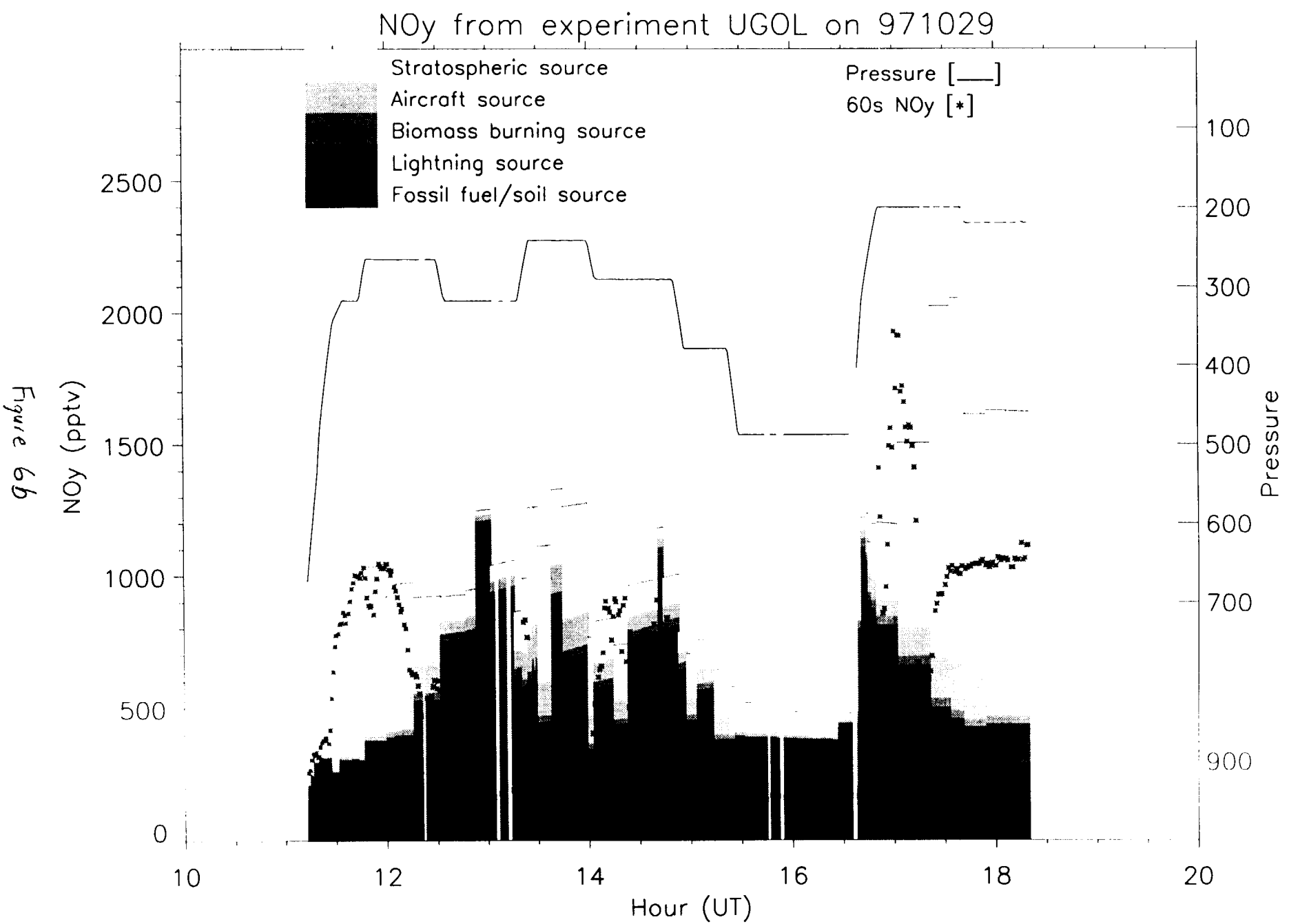
NOy from experiment UGOL on 971029
Stratospheric source
Aircraft source
Biomass burning source
Lightning source
Fossil fuel/soil source
Pressure [___]
60s NOy [*]
NOy (pptv)
Pressure
Hour (UT)
2500
2000
1500
1000
500
0
100
200
300
400
500
600
700
900
10
12
14
16
18
20

Figure 66

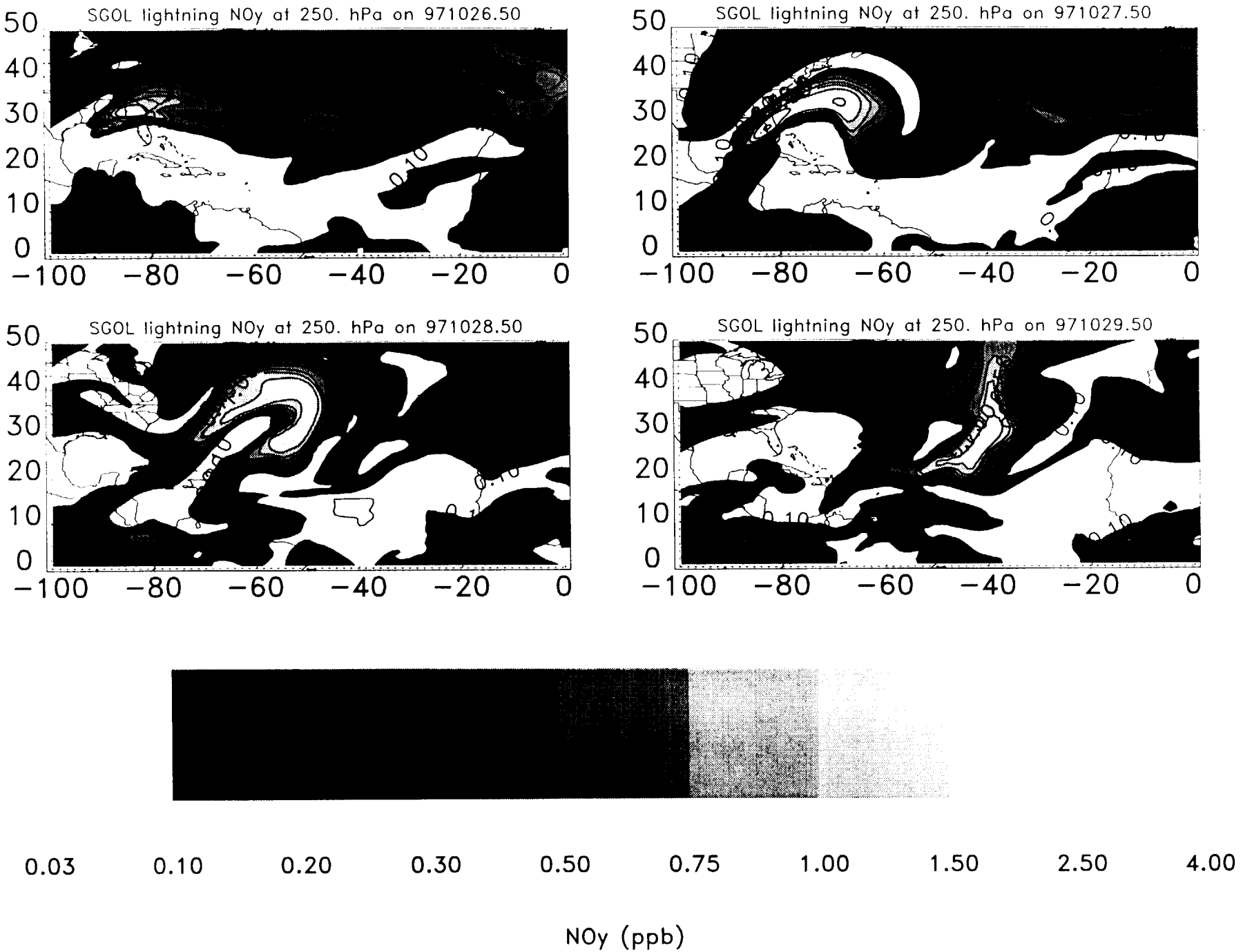
SGOL lightning NOy at 250. hPa on 971026.50
SGOL lightning NOy at 250. hPa on 971027.50
SGOL lightning NOy at 250. hPa on 971028.50
SGOL lightning NOy at 250. hPa on 971029.50
50
40
30
20
10
0
−100
−80
−60
−40
−20
0
0.03
0.10
0.20
0.30
0.50
0.75
1.00
1.50
2.50
4.00
NOy (ppb)

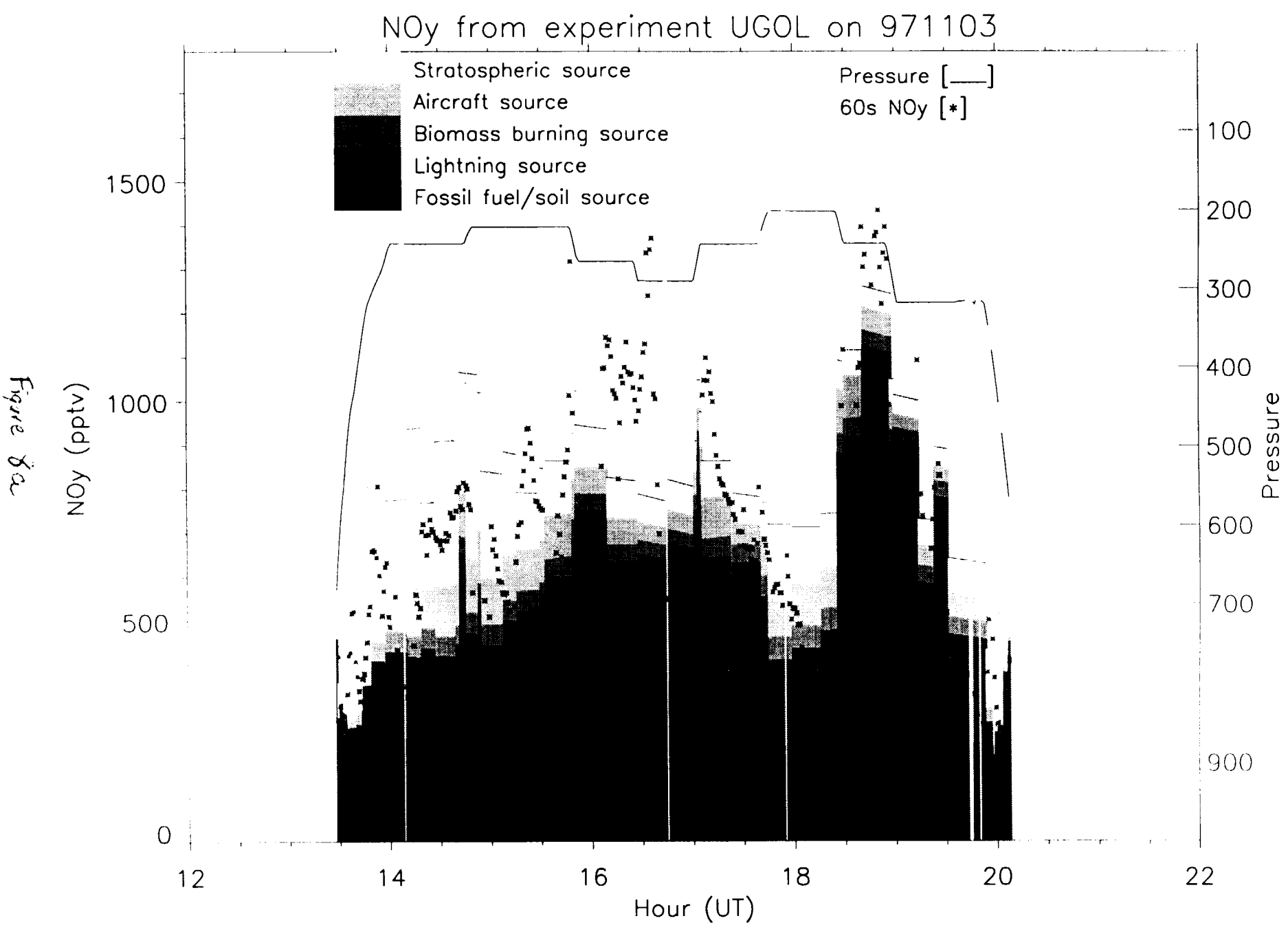
NOy from experiment UGOL on 971103
Stratospheric source
Aircraft source
Biomass burning source
Lightning source
Fossil fuel/soil source
Pressure [___]
60s NOy [*]
NOy (pptv)
1500
1000
500
0
Pressure
100
200
300
400
500
600
700
900
12
14
16
18
20
22
Hour (UT)

Figure 3a

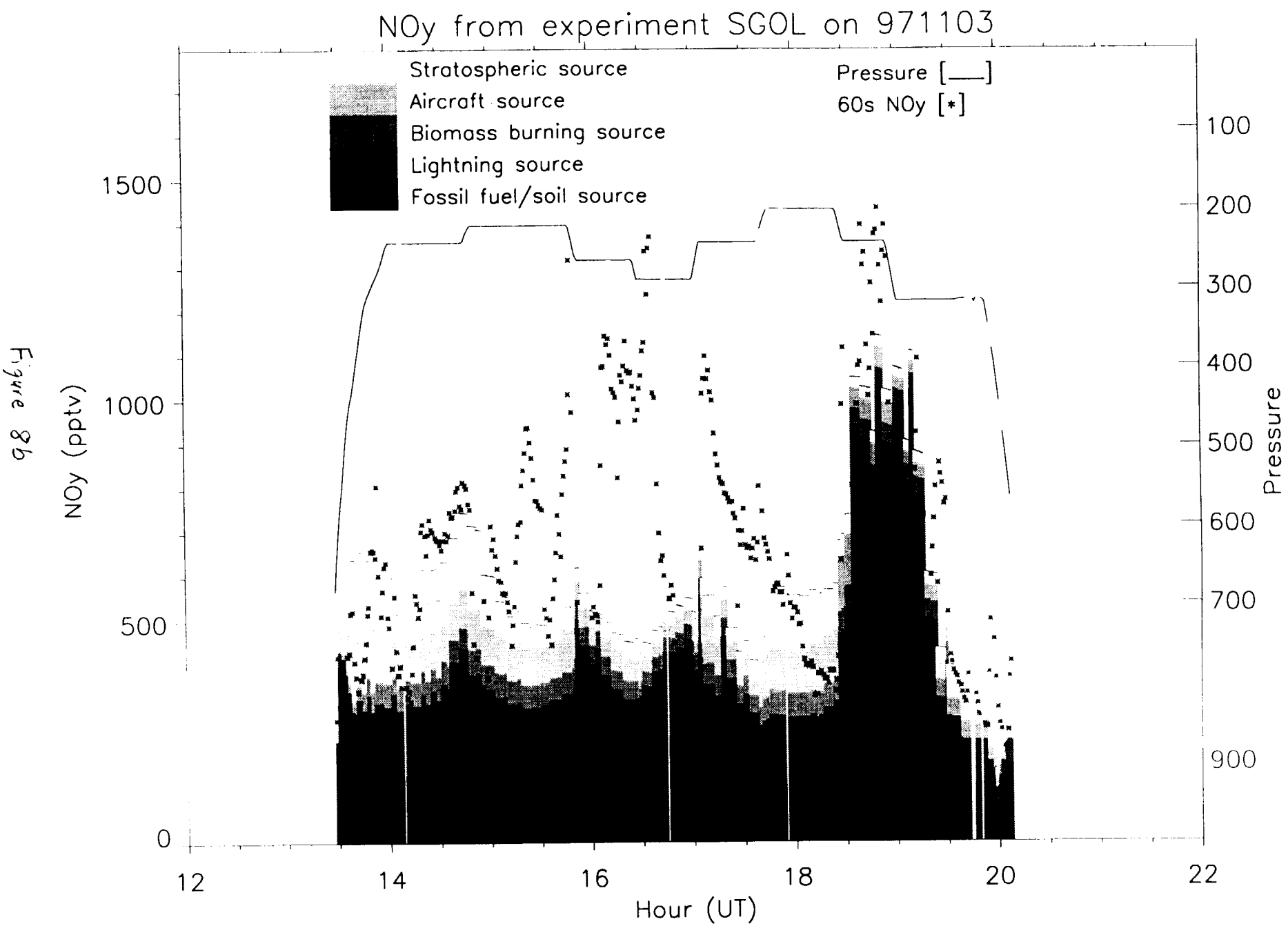
NOy from experiment SGOL on 971103
Stratospheric source
Aircraft source
Biomass burning source
Lightning source
Fossil fuel/soil source
Pressure [___]
60s NOy [*]
NOy (pptv)
Pressure
Hour (UT)
0
500
1000
1500
100
200
300
400
500
600
700
900
12
14
16
18
20
22

Figure 8b

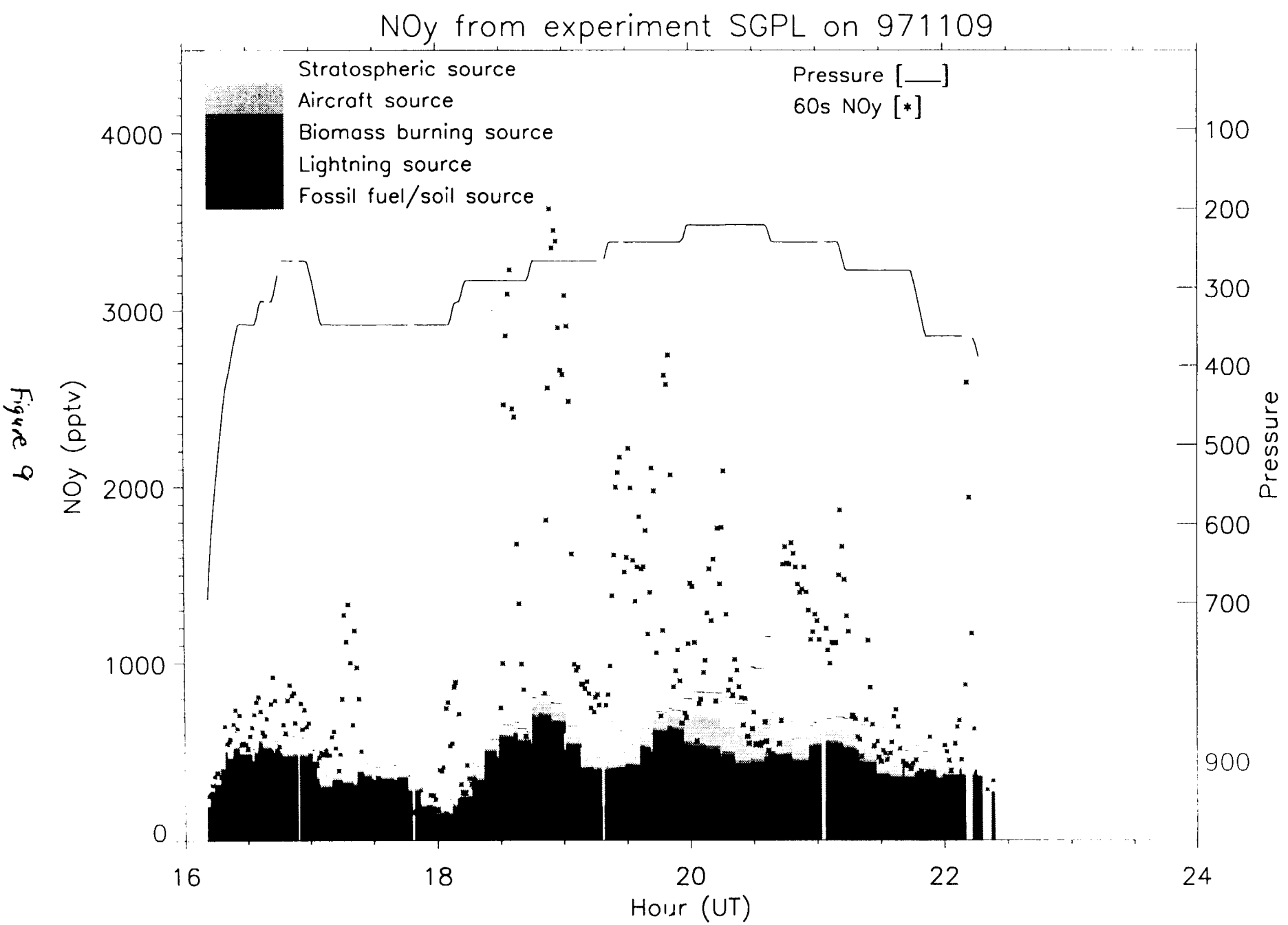
NOy from experiment SGPL on 971109
Stratospheric source
Aircraft source
Biomass burning source
Lightning source
Fossil fuel/soil source
Pressure [___]
60s NOy [*]
NOy (pptv)
Pressure
Hour (UT)
0
1000
2000
3000
4000
100
200
300
400
500
600
700
900
16
18
20
22
24

Figure 9

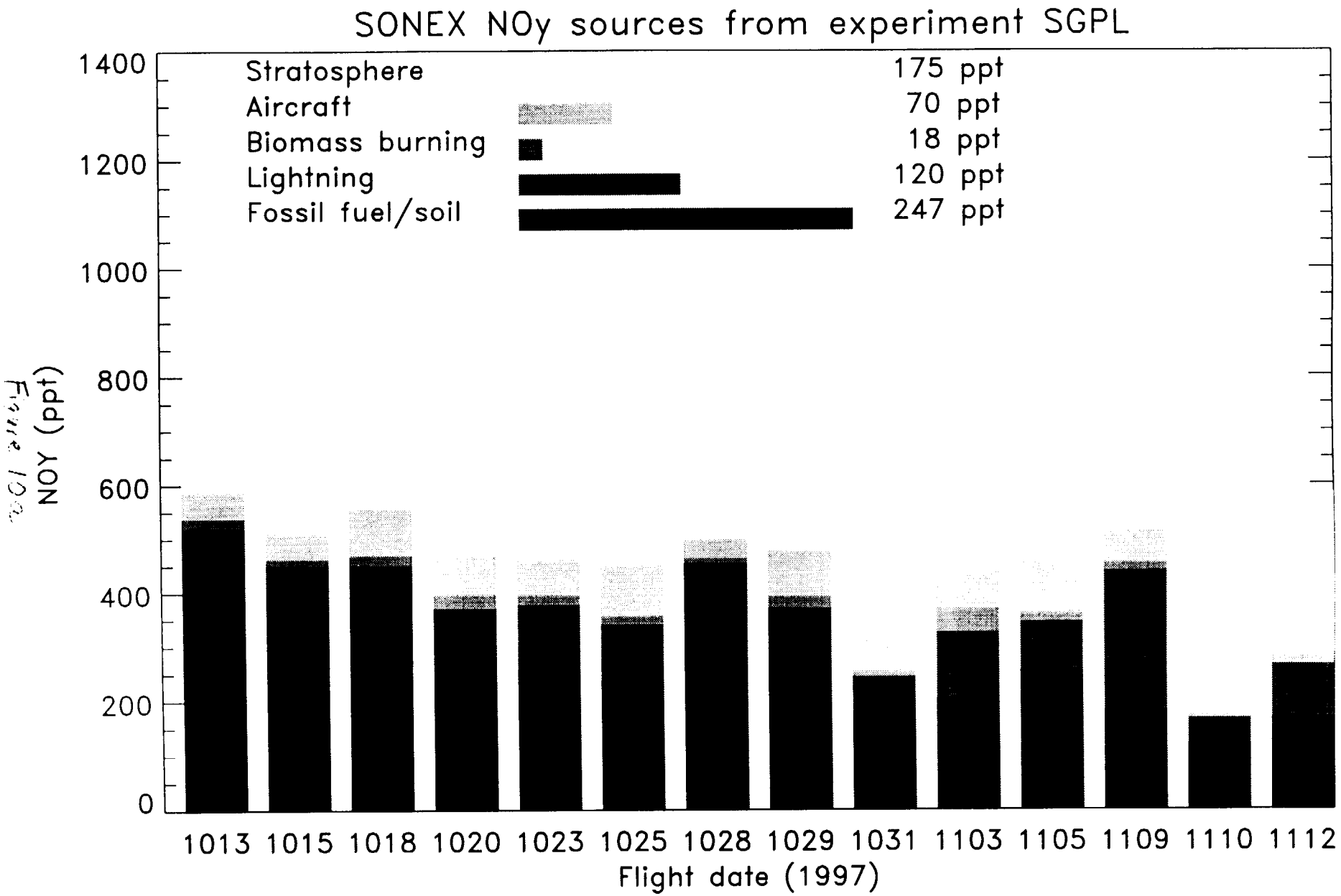
SONEX NOy sources from experiment SGPL
Stratosphere 175 ppt
Aircraft 70 ppt
Biomass burning 18 ppt
Lightning 120 ppt
Fossil fuel/soil 247 ppt
NOY (ppt)
0
200
400
600
800
1000
1200
1400
1013 1015 1018 1020 1023 1025 1028 1029 1031 1103 1105 1109 1110 1112
Flight date (1997)

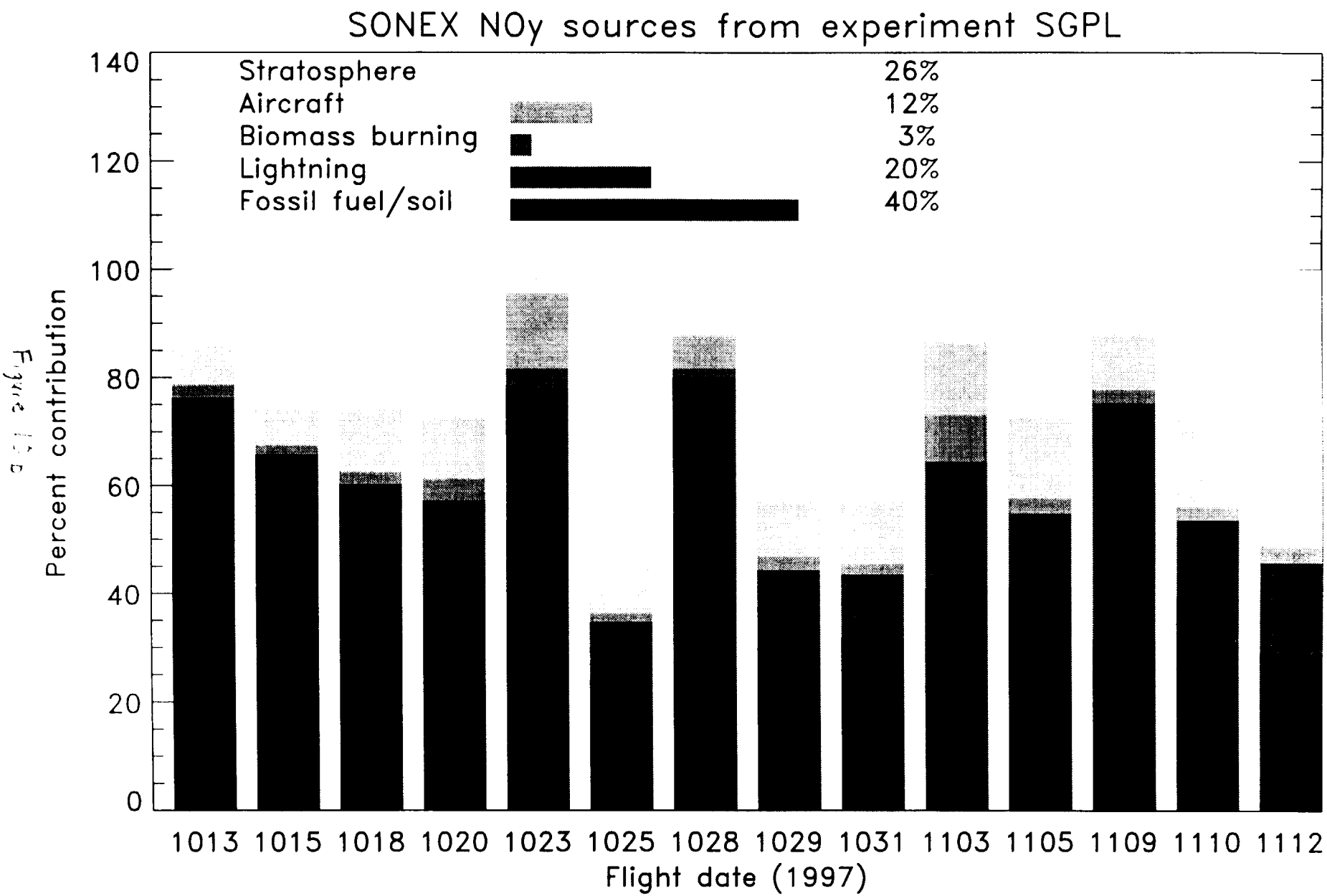
SONEX NOy sources from experiment SGPL
Stratosphere 26%
Aircraft 12%
Biomass burning 3%
Lightning 20%
Fossil fuel/soil 40%
Percent contribution
0
20
40
60
80
100
120
140
1013 1015 1018 1020 1023 1025 1028 1029 1031 1103 1105 1109 1110 1112
Flight date (1997)

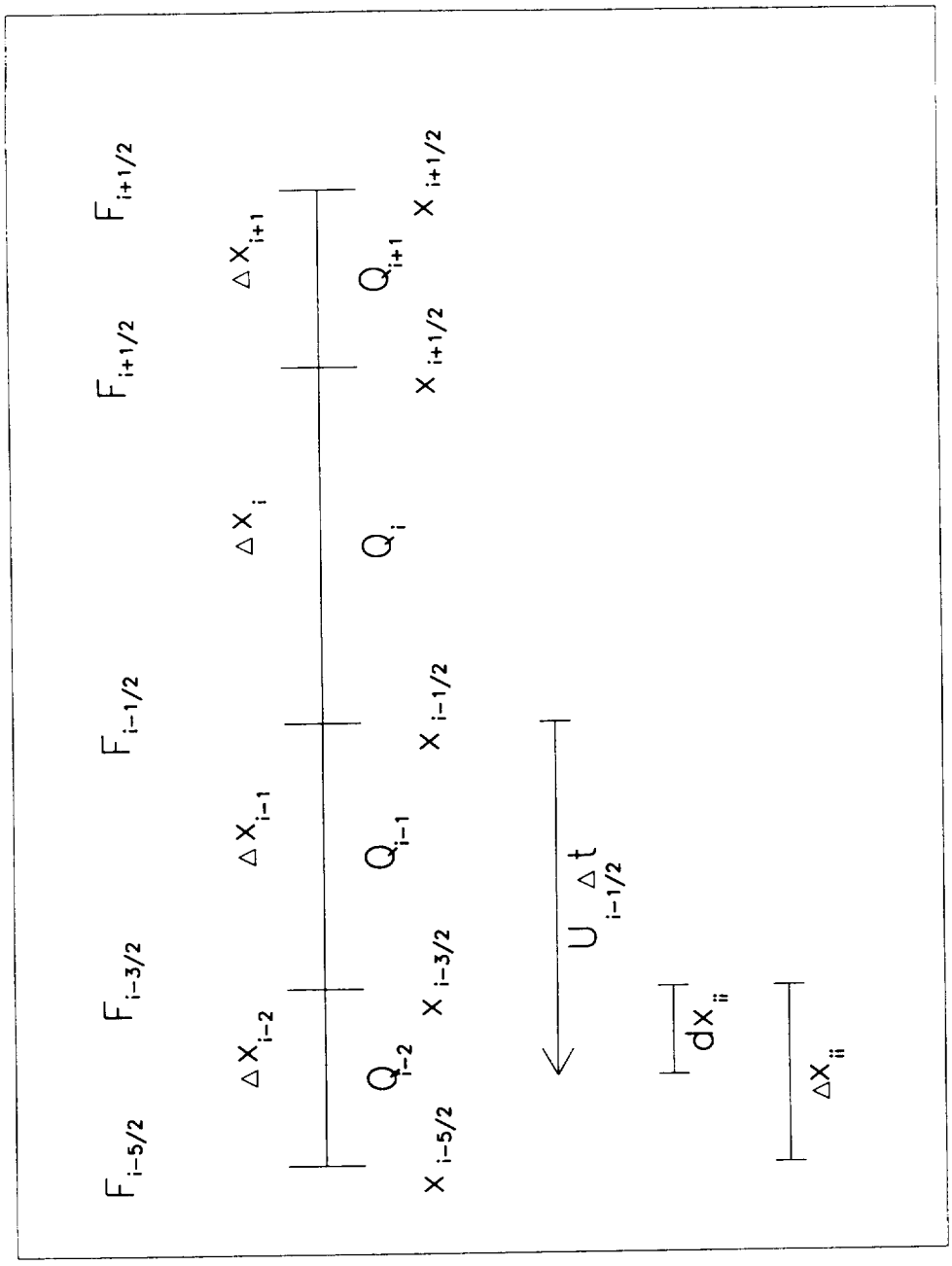
F i-5/2
F i-3/2
F i-1/2
F i+1/2
F i+1/2
Δ X i-2
Δ X i-1
Δ X i
Δ X i+1
Q i-2
Q i-1
Q i
Q i+1
X i-5/2
X i-3/2
X i-1/2
X i+1/2
X i+1/2
U Δ t
i-1/2
dx ii
Δx ii

Figure A1